ABSTRACT

Title of thesis:	ANALYSIS AND MEASUREMENT OF CANDLE FLAME SHAPES
	Gregory A. Tabaka, Master of Science, 2008
Thesis directed by:	Assistant Professor Peter B. Sunderland Department of Fire Protection Engineering

A combined analytical and experimental study was performed to produce and validate a method by which the lengths and widths of flames burning on wax candles can be predicted. Two analogies are drawn: first, that heat transfer from the wick can be modeled as a slender vertical rod undergoing a natural convection process surrounded by a stagnant film; and second, that fuel pyrolyzed from the wick surface that remains unburned until above the wick can be modeled as flow from a circular port burner. Empirical correlations applied to the theoretical equations have produced reasonable agreement with measured flame lengths and widths for paraffin candles.

ANALYSIS AND MEASUREMENT OF CANDLE FLAME SHAPES

by

Gregory A. Tabaka

Thesis submitted to the Faculty of the Graduate School of the
University of Maryland, College Park in partial fulfillment
of the requirements for the degree of
Master of Science
2008

Advisory Committee:
Professor Peter B. Sunderland, Chair
Professor James G. Quintiere, Co-Chair
Professor Arnaud Trouvé

Dedication

To Thomas Jefferson, patron saint of freedom and architect of American liberty.

Acknowledgements

As most any graduate student laments, the academic process of writing a thesis takes longer than anticipated and requires the touch of other people to become successful. Few of us have the capacity to make discoveries and change the world in isolation like Isaac Newton. I am no exception and feel the need to express my gratitude towards those who have contributed to completing this paper.

First, I would like to thank my thesis advisors at the University of Maryland, College Park, professors Peter B. Sunderland and James G. Quintiere. Their willingness to advise a student without outside funding bespeaks their devotion to the pursuit of knowledge and discovery. Their tutelage was central to pouring the theoretical foundation of this work and their subsequent efforts allowed it to grow into something substantial and contributory to the body of combustion literature, yet they provided the broad measure of independence and freedom I required to make this thesis the fruits of my own labor.

The experimental data were graciously provided by Danjun Lian while in the United States during a brief junket away from life in China. Her observation and digitization of candle flame shapes allowed me to not only validate the theory presented herein but also to demonstrate trends that I did not anticipate. If one good experiment is worth the opinion of a thousand experts, then her thirty good experiments are worth far more than the solitary opinion of this student.

I owe a large debt of gratitude to Dr. Javier Trelles, who graciously donated his time to help my understanding of axisymmetric flows, combustion within annular

structures, the numerical mathematical techniques that ultimately did not make it into this thesis and—most of all—for academic direction when I was wandering.

Also, I wish to thank Dr. Arnaud Trouvé of the University of Maryland, College Park particularly for serving on my thesis defense committee. I also thank him for lecturing the graduate *Diffusion Flames and Burning Rates Theory* class, which served as excellent preparation for the subject matter of this thesis.

In a similar vein, I thank the professors at the University whom I have not yet mentioned for their instruction throughout the years and for preparing me for the profession of fire protection engineering: André W. Marshall, Marino di Marzo, James A. Milke and Frederick W. Mowrer. In fact, if Dr. di Marzo had not spoken to my class about the Graduate School, I would not have made the decision to pursue a Master's degree.

Also, I wish to thank my friends and family for their encouragement, patience and ability to preserve my sanity. This thesis was researched and written largely while on long business trips away from home that endured for months at a time. The ability to come home and rejoin my friends and family has made all the difference.

Greg Tabaka
November 9, 2007
Airborne somewhere between Tampa and Baltimore

Table of Contents

List of Tables

List of Figures

Nomenclature

Latin symbols

B	Spalding B number (unitless)
c_p	Specific heat of gas at constant pressure at T_m (J/kg·K)
C_0	Axial velocity modulus ($m^{1/2}/s$)
C_1	Axial velocity scaling factor (unitless)
D	Diameter of the wick at the vertical midpoint (m)
$\mathcal{D}$	Diffusion coefficient (m^2/s)
emp	Empirical fit
f	Mixture fraction (unitless)
g	Gravitational acceleration (m/s^2)
Gr_x	Grashof number $= g\mu\Delta T x^3/\nu^2$ (unitless)
h	Heat transfer coefficient (W/m^2·K) or enthalpy (J/kg)
H	Enthalpy of gasification (J/kg·K)
k	Thermal conductivity at T_m (W/m·K)
L	Length of wick from the molten pool to the wick tip (m)
m	Mass (kg)
M	Molecular weight (kg/mol)
n	Empirical data fit parameter (unitless)
Nu_x	Nusselt number $= hx/k$ (unitless)
Pr	Prandtl number $= \nu/\alpha$ (unitless)
r	Radial coordinate (m)
R	Radius of the wick (m)
Ra_x	Rayleigh number $= \mu_m (T_f - T_\infty) x^3/\mathrm{Pr}\,\alpha_m^2$ (unitless)
s	Stoichiometric fuel-oxygen mass ratio (unitless)
S	Stoichiometric fuel-air molar ratio (unitless)
T	Temperature (K)
w	Maximum diameter of the flame (m)
u	Axial component of velocity (m/s)
V	Volume (m^3)
v	Radial component of velocity (m/s)
X	Mole fraction (unitless)
Y	Mass fraction (unitless)
y	Standoff distance from wick surface (m)
z	Axial coordinate (m)

Greek and other symbols

α	Thermal diffusivity (m^2/s)
β	Similarity variable (J/g)
δ	$= R + y_\delta$; Velocity boundary layer position (m)
θ_x	Difference variable (for $x = T$: K, for $x = \{$ F, Ox, N, P $\}$: unitless)
Θ	Stretched coordinate (see [1])
λ	Dimensionless mass flow per unit height $= \dot{m}'_F/\psi$ (unitless)
μ	Thermal volumetric expansion coefficient (1/K)
ν	Kinematic viscosity (m^2/s)
ρ	Mass density (kg/m^3)
ψ	$= 2\pi k/c_p = 2\pi\rho\mathcal{D}$
Δh_c	Enthalpy of combustion (J/kg)

Subscripts

0	Reference state of formation (superscript)
b	Relating to the apparent circular port burner
B	Burned
D	Wick diameter
E	Entrained
F	Fuel
f	Flame sheet
g	Gas
l	Liquid
L	Wick length
m	Fuel/products region between wick surface and flame sheet
N	Inert diluent
Ox	Oxygen
P	Product of combustion
v	Vaporization of liquid fuel
∞	Ambient
δ	Boundary layer

Superscripts

$\dot{x}$	x per unit time (x/s)
x'	x per unit wick length (x/m)
x''	x per unit surface area (x/m^2)
x'''	x per unit surface volume (x/m^3)
x^*	x is nondimensional (–)

Chapter 1

Introduction

The candle flame has formed a fundamental basis in the study of fire and has enlightened researchers about the nature of steady laminar flames, soot production, burning rates, and combustion in microgravity amongst other topics. An improved understanding of the candle flame itself may further the state of the art and lead to other advances in combustion and fire science. For instance, simplified analytical methods such as that posed within can be used to validate more complex code or provide valuable estimation or design techniques. This analysis can also be extended to other geometries or gravitational conditions where data exist about free-convective heat transfer. Candle research can lead to reduced frequency of fires and soot emissions in homes. It can also be used by manufacturers to select wax and wick properties to obtain desired flame widths, lengths and luminosities.

One of the earliest studies of candle flame dynamics was presented in 1860 by Michael Faraday [2]. More recent scholarship on wicked candles began *circa* 1990 and has continued since. These studies were primarily simplified numerical studies, themselves representing the solution of a simplified set of equations of motion. This facilitated solution by computer, which is why the timeframe coincides with the rising popularity of the personal computer.

However, if we generalize our study to flames on vertical surfaces (with a con-

centration on vertical cylinders), the body of research swells.

Multiple studies exist for burning under forced convection. Emmons' [3] seminal paper studied combustion of burning droplets with forced convection and obtained a similarity solution, assuming a stagnant boundary layer. The approach taken by Emmons would be influential in subsequent analyses. Also, the coupling of convective effects with stagnant films used by Spalding [4] and Emmons was also influential in this field of study. Abdel-Khalik et al. [5, 6] studied horizontal cylinders of porous material saturated with n-heptane under forced convection as an approximation to droplet burning. Tao and Kaviany [7] and Tao et al. [8] studied the burning rate of fuel supplied to a porous slab under forced convection.

Several studies exist for free convection as well, for a variety of liquid and solid fuels. Kaviany and Tao [9] studied vaporization effects on a liquid-soaked block of porous material in free convection. Raju and T'ien [10] experimentally studied heat and mass transport within porous planar wicks. Kim et al. [11] studied laminar burning on vertical, horizontal and inclined geometries saturated with liquid fuel and obtained an approximate solution for burning rate based on the Grashof and Spalding B numbers, albeit employing theory that neglects wick curvature effects. Kosdon et al. [12] studied burning of alpha-cellulose vertical cylinders under laminar, free-convective conditions and obtained a scaling law for flame standoff distance as a function of vertical position. Ahmad and Faeth [13] analyzed liquid burning on a vertical planar surface, but also studied the flame shape in a region where no fuel is being added, which is similar to the region above a candle wick. Malary and Sibulkin [14] examined laminar burning of methyl methacrylate (a solid material

with favorable chemical decomposition behavior) of vertical flat plates and found that a unique burning rate did not exist. Groff and Faeth [15] explored a liquid-fueled wick fed by reservoir otherwise geometrically similar to a candle but they worked in rectilinear coordinates. Maxworthy [16] examined the instability of propane flames using a burner whose form is very similar to the wick of Groff and Faeth [15].

Pagni [17] presented nine "classic" diffusion flames with theoretical solutions, including a cylindrical stagnant layer solution similar to the analysis presented within this thesis. Pagni was able to relate the width of the flame to the mass burning rate but did not express his solution in terms of practical dimensionless groups. He was able to obtain an expression for flame height by treating fuel unburned until above the fuel source to be flow from a Burke-Schumann burner but presented his results as a curve fit in thermophysical and chemical quantities.

A number of studies in microgravity were performed as well. Linan [18] studied burning of solid fuel cylinders in microgravity. Dietrich et al. [19, 20] studied candle flames in microgravity and non-buoyant atmospheres, in which molecular diffusion is shown to be the governing phenomenon. Du et al. [21] performed experiments to measure the temperatures of candle flames in microgravity.

In the past two decades, several computational fluid dynamics analyses have been made. Lyu and Chen [22] performed a numerical study of planar and cylindrical liquid-fueled porous wicks that demonstrated that the fuel vaporization rate on cylinders deviated from the $z^{-1/4}$ dependence for flat plates, where z is distance in the vertical direction. Wu and Chen [23] applied a mixture fraction approach to study the shape and oscillation of near-laminar flames on cylindrical wicks by

numerical solution of a system of partial differential equations (PDE). Riley [24] created a PDE model using the flame sheet model for steady burning on candle wicks much longer than the flame itself, though he predicted only the steady state of the system. Hamins et al. [25] used Fire Dynamics Simulator (FDS) from the National Institute of Standards and Technology (NIST) to model a candle flame, including the bent geometry of a wick. Alsairafi et al. [26, 27] created a detailed computational fluid dynamics model of a candle flame with chemical kinetics, assuming that the wick surface was saturated with liquid fuel and studied the effect of varying gravitational accelerations. Raju [28] incorporated a model of heat and mass flow within a candle wick into Alsairafi's computational model to remove the saturated surface assumption and to numerically study heat and mass transport within the wick, thereby adding a direct coupling mechanism between flame and fuel supply.

Literature pertaining to heat transfer or gaseous combustion has been omitted in this history. This thesis will base burning behavior on heat transfer literature and extend the process to combustion. Specifically, the processes of natural convection along vertical cylinders and burning from circular gaseous port burners are employed.

In particular, this thesis proposes a methodology for predicting the width, length and burning rate of a paraffin candle flame as the geometry of the wick—namely, length and diameter—changes. The effect of variation in fuel is not experimentally explored, though the method does allow for chemical effects to be included through the concepts of stoichiometry, B number and transport rates.

Thus motivated, the objectives of this study are as follows:

1. Predict the widths of candle flames;

2. Predict the lengths of candle flames; and

3. Compare predicted quantities against experimental observations.

This thesis will begin by describing the experimental data gathering scheme that was implemented by Dan-jun Lian, which led to the validation set for the analytical method that follows. This analytical approach can best be described as an approximate treatment based on the heat transfer literature with a classical application of fluid mechanics and combustion theory. The analysis extends the burning rate and flame sheet treatments presented in Quintiere [29] to cylindrical coordinates to produce scaling laws. A further chapter is devoted to discussing the accuracy and limitations of the formulae created, as well as possible extrapolation to conditions different than those tested. Finally, measurements are presented for substantiation and for later researchers to utilize.

Chapter 2

Experimental

Laboratory experiments were conducted in which five different diameters of wick were molded into paraffin candles with various lengths of wick exposed above the plane of wax that forms the top of the candle. The candle was then set on a bench, ignited and observed. When steady state burning was achieved (as evidenced by the formation of a liquid pool of 25 mm in diameter), a high resolution photograph was taken for later measurement on a personal computer. No measurements of mass loss, temperature or velocity were obtained as the purpose was only to determine the extent of the luminous region of flame under the assumption that the wick geometry would be the governing influence.

2.1 Procedure

The experimental procedure that was followed is described below and is similar to that used previously in this laboratory to measure candle smoke points by Allan et al. [30].

1. Prepare the candle.

    (a) Cut wick to desired length.

    (b) Place paraffin beads into a beaker that serves as the mold for the candle.

(c) Melt paraffin beads and allow to solidify.

(d) Remove from beaker.

(e) Drill hole on axis.

(f) Stiffen wick by adding liquid wax.

(g) Insert wick into hole.

2. Position camera to obtain a clear photograph.

3. Light the candle and place it inside a Plexiglas draft shield.

4. Wait for the candle to achieve a laminar, stable burning regime.

5. Snap the photograph with the Nikon D100 digital camera.

6. Record observation notes and photograph serial number.

2.2 Flame Shape Measurements

Once the catalog of photographs has been uploaded to a personal computer, they were analyzed to obtain flame measurements. Once the image in question is on screen, the measurement of interest (e.g., flame width) is taken in pixels. Because the scaling factor between pixels and physical distance is known, the actual distance represented on screen can be measured. Using this technique, all 33 flame photographs were measured. The following measurements were recorded:

1. Height of the flame attachment point above the wax pool

2. Length of the wick above the molten wax pool, L

3. Diameter of the wick at the vertical midpoint, D

4. Diameter of the wick at the top

5. Dry wick diameter using a caliper with minimal force applied

6. Length from the molten wax pool to the flame tip

7. Maximum diameter of the flame, w

Mass loss rates were not recorded.

The described technique offers several benefits. First, all dimensions of the flame are available at one particular instant in time. That is, the width and length are presented as a couple, rather than having been measured sequentially, introducing error. Second, measuring the width of a flame directly is difficult and may affect gas flow or introduce cooling effects, which could influence the measurement. Third, an electronic record is made that can be checked in the future. Finally, the high resolution camera produces images that can be measured very precisely. A conversion factor of one millimeter per 33.95 pixels was employed, so measurements should have an accuracy of one half-pixel ($\pm$ 0.059 mm); however, the actual error in measurement is significantly higher.

The source of this error is threefold: first, the base of the candle flame as measured has a faint blue corona that does not appear clearly in digital photographs and makes discerning the flame attachment point particularly difficult. Second, despite attempts to produce steady flames, flicker and drafts still do occasionally coincide with the photograph. Third, the physical endpoints to measurements are some-

times difficult to discern, especially in flame regions that are not sharply defined. One cause of the nonexistence of ideal measurement points can be attributed to the fact that the wick could not always be aligned perfectly to gravity, nor do candle wicks have the uniform cylindrical shapes with constant diameters and plane ends that theorists apply to simplify the mathematics.

The raw data was compiled to a spreadsheet application. This electronic format provided enough flexibility to be able to store, transmit, manipulate, calculate and plot results to gain qualitative and quantitative understandings of candle flame behaviors.

Chapter 3

Candle Flame Shape Theory

Previous analyses of flame structure have been attempted on a broad spectrum of theory: some are simplistic one-dimensional analyses with planar flames; some have attempted direct numerical simulation using detailed information on elaborate chemical reaction kinetics and flow phenomena; still others utilize a blend of science rooted in fundamentals and a pragmatic empiricism to obtain solutions. This thesis can comfortably claim to be in the lattermost category.

The most fundamental approach encountered within the literature is to conceptualize a saturated, porous fuel source with a flame attached and attempt to solve the boundary layer equations in rectilinear coordinates. This approach was followed by Kim et al. [11], Ahmad and Faeth [13], and Groff and Faeth [15]. This thesis will depart from their strategy by referencing the boundary layer equations mainly for the purpose of calculating upward mass flow but will retain the porous fuel source component. Instead of solving the boundary layer equations or computing the flow field such as Lyu and Chen [22], Wu and Chen [23], Riley [24], Alsairafi [26, 27], and Raju [28] have done, this paper will employ a heat transfer correlation and stoichiometry to quantify upward fuel flow. This semi-empirical approach is employed because—unlike Emmons [3]—a similarity solution for the problem of a flame within stagnant film does not exist for a vertical cylinder, thereby limiting the methods of

solution available. This approach was deemed to be more amenable to producing scaling law relationships than CFD studies and therefore was chosen. Also, the flame height is calculated via correlation rather than as a result of a flow field computation. This flame height calculation is reminiscent of Pagni's [17] approach in which he assumed fuel not burned lateral to the wick entered a Burke-Schumann [31] port burner above.

The analytical theory presented here begins by making an analogy between a candle flame and a slender vertical rod undergoing natural convective cooling for the purposes of calculating the mass flux of fuel through the wick surface along the vertical face. More precisely, the mass transfer rate due to vaporization is coupled to heat transfer. Next, stoichiometry and stagnant laminar boundary layer theory are employed to approximate the mass flow rate of oxidizer joining the flame front. Knowing the amount of fuel vaporized and the amount of oxidizer available, it is possible to calculate the amount of fuel that remains unburned in the lateral region and is therefore transported to the overwick region for eventual combustion. It is hypothesized from experimental observation that the maximum flame diameter resides at this interface. The vertical flow of fuel there resembles a circular port gaseous fuel burner and so flame height is calculated using literature available on that topic. The candle, flame and geometry described above are shown schematically in Fig. 3.1. The theory is then adjusted empirically to improve the agreement between theory and observed fact.

This methodology presented relies on several key assumptions:

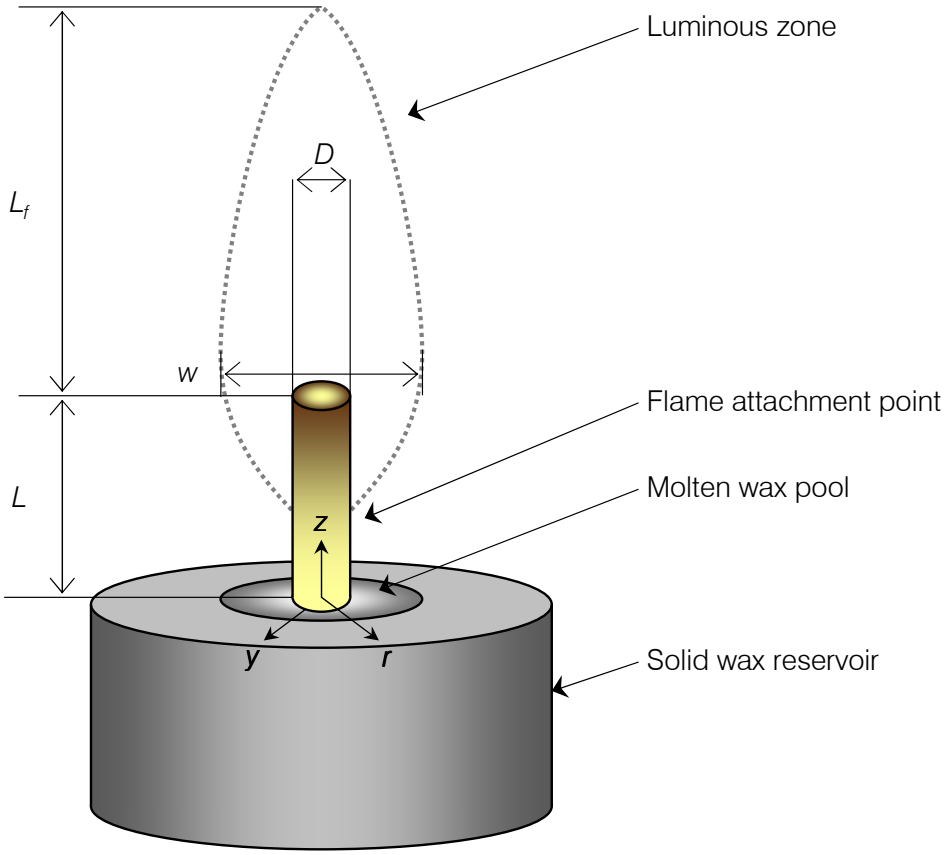

Figure 3.1: Candle and flame schematic

1. The heat transfer from the flame to the wick can be modeled as a vertical cylinder at flame temperature cooling under the influence of natural convection without a surrounding flame front;

2. Pyrolyzate that has not burned laterally to the wick can be modeled as fuel flowing vertically from a circular port burner;

3. Compressibility effects can be ignored;

4. The flame and near flow field remain steady, laminar and axisymmetric;

5. The wick is shaped as a cylinder and remains uniformly saturated with liquid fuel at the surface; and

6. The fuel is burned in stoichiometric proportions with oxidizer.

3.1 Boundary Layer Flow

Central to this paper is the hypothesis that a candle flame can be modeled as residing within a stagnant laminar boundary layer where the fuel vaporization rate is coupled with heat conduction. In this idealized model, the candle wick is perfectly cylindrical and aligned parallel to the gravity vector and is therefore axisymmetric. In Fig. 3.2, the dashed curve schematically represents the boundary layer known to classical heat transfer as the stagnant boundary layer and the solid curve represents the candle flame sheet. Specifically, the stagnant boundary layer has a thickness proportional to the quarter power of the vertical coordinate [32] (i.e., $y_\delta \propto z^{1/4}$) and the flame lies at some fraction of this thickness, as will be shown.

The natural point of departure for this analysis is a consideration of the flow within the boundary layer. We can express the mass flow rate in the z-direction by abstractly integrating the upward mass flux, $\dot{m}''$, as

$$\dot{m}(z) = \int_R^\delta \dot{m}''(r, z)\, dA, \tag{3.1}$$

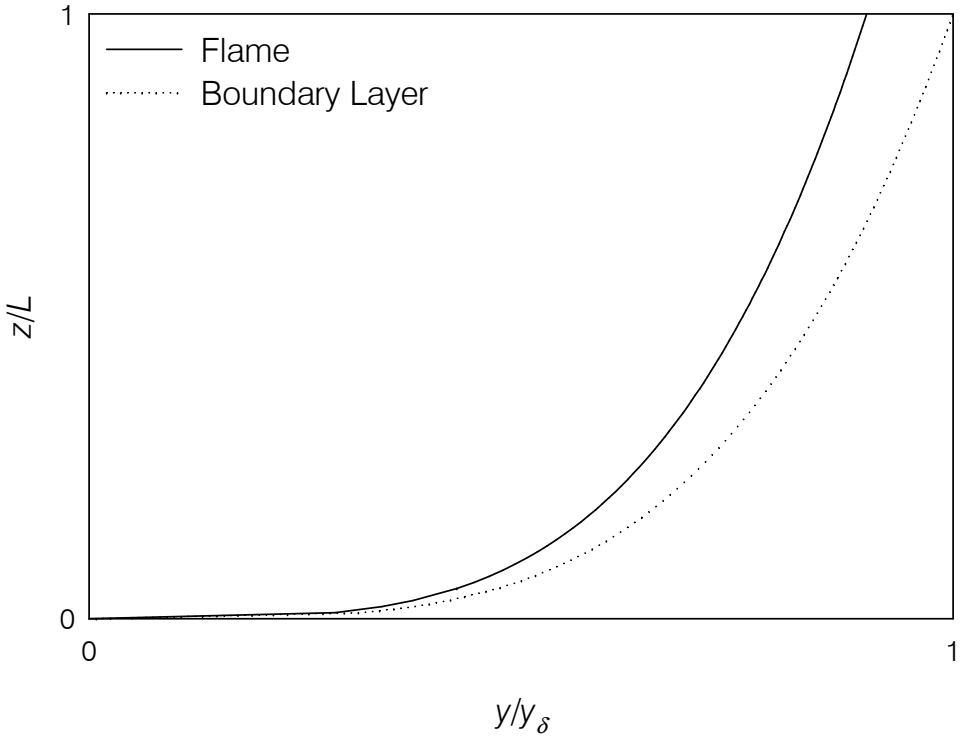

Figure 3.2: Qualitative stagnant boundary layer profiles for a slender vertical rod undergoing natural convective cooling (dashed) and for a candle flame (solid) below the top of the wick.

or, more concretely, while emphasizing the cylindrical nature of the problem as

$$\dot{m}(z) = 2\pi \int_{R}^{R+y_\delta} \dot{m}''(r,z)\, r\, dr. \tag{3.2}$$

For tractability, we assume a constant density of ρ_m, which represents the average density of the region between the wick surface and flame sheet at a given axial coordinate, z. This value for density has been chosen because this region occupies the majority of the space between the wick and the thermal boundary layer (as will

be shown later). By substituting $\dot{m}'' = \rho_m u(r,z)$, we can approximate the mass flow rate as

$$\dot{m}(z) = 2\pi\rho_m \int_R^{R+y_\delta} u(r,z)\, r\, dr. \tag{3.3}$$

To obtain an estimate of the proportions of fuel and oxidizer that comprise $\dot{m}(z)$, we realize that $\dot{m}(z)$ reflects the sum of mass flow from fuel vaporized from the wick surface and the air entrained to combust that fuel (recall that the boundary layer extends beyond the flame sheet, so the presence of air between the limits of integration is still consistent with the flame sheet model). The total vertical mass flow within the boundary layer at the top of the wick can be expressed as

$$\dot{m}(L) = \int_0^L \left(\dot{m}'_{F,z} + \dot{m}'_{E,z}\right)\, dz = \dot{m}_{F,L} + \dot{m}_{E,L}. \tag{3.4}$$

For candle flames that extend beyond the top of the wick, we can conclude that some fuel vaporized from the wick remains unburned in the lateral region and it therefore becomes interesting to calculate this quantity. To do so, we assume fast chemistry to achieve stoichiometric burning and a uniform mass fraction of oxygen in air. Further, we assume that all air entrained in the lateral region is consumed there and is not transported to the overwick region. Thus, the stoichiometric burning rate of fuel in the lateral region is given by

$$\dot{m}_{F,B} = \frac{\dot{m}_{\mathrm{Ox},E,L}}{s} \tag{3.5}$$

and the mass flow rate of oxidizer is given by

$$\dot{m}_{\mathrm{Ox},E,L} = Y_{\mathrm{Ox},\infty}\dot{m}_{E,L}. \tag{3.6}$$

By combining Eqs. 3.5 and 3.6, we can quantify the amount of fuel transported to the overwick region to be

$$\dot{m}_{F,\delta} = \dot{m}_{F,L} - \dot{m}_{F,B} = \dot{m}_{F,L} - \frac{Y_{\mathrm{Ox},\infty}\dot{m}_{E,L}}{s}. \tag{3.7}$$

By Eq. 3.4, we can rewrite this as

$$\dot{m}_{F,\delta} = \dot{m}_{F,L}\left(1 + \frac{Y_{\mathrm{Ox},\infty}}{s}\right) - \frac{Y_{\mathrm{Ox},\infty}}{s}\dot{m}(L). \tag{3.8}$$

This equation is still incomplete and requires an expression for $\dot{m}_F$ and some representation of the axial velocity profile for $\dot{m}(L)$ included through Eq. 3.3.

3.2 Fuel Vaporization

To produce an expression for the sidewall fuel vaporization rate, $\dot{m}_F$, we begin with a simplified set of conservation equations expressed in cylindrical coordinates for axisymmetric flow [33]:

$$-\sum h^0_{f,j}\dot{m}'''_j = \frac{1}{r}\frac{\partial}{\partial z}\left(r\rho u\int_{T_0}^{T} c_p(T)\,dT\right) + \frac{1}{r}\frac{\partial}{\partial r}\left(r\rho v\int_{T_0}^{T} c_p\,dT\right) - \frac{1}{r}\frac{\partial}{\partial r}\left(r\rho\mathcal{D}\frac{\partial}{\partial r}\int_{T_0}^{T} c_p\,dT\right) \tag{3.9}$$

$$\dot{m}_j''' = \frac{1}{r}\frac{\partial}{\partial z}\left(r\rho u Y_j\right) + \frac{1}{r}\frac{\partial}{\partial r}\left(r\rho v Y_j\right) - \frac{1}{r}\frac{\partial}{\partial r}\left(r\rho\mathcal{D}\frac{\partial Y_j}{\partial r}\right) \tag{3.10}$$

in which $\dot{m}_j'''$ is defined as the rate of *production* of species j and a Lewis number of unity was assumed, so $\rho\mathcal{D} = k/c_p$.

For the purpose of calculating the mass flow of fuel vaporizing from a wick, we will apply additional simplifications. First, we approximate $\int_{T_0}^{T} c_p(T)\,dT = c_p\left(T - T_0\right)$ with c_p held constant to remove the integral in Eq. 3.9. Next, we assume that the first terms in Eqs. 3.9 and 3.10 are negligible in comparison to the others on the basis that temperature, mass fraction and velocity gradients in the axial direction are small in comparison to those in the radial direction. Indeed, the temperature and mass fraction of the wick surface are assumed to be uniform and at the boiling point and saturation concentration of the fuel and is assumed to have an axial velocity near zero. The large effect of this assumption is to remove any dependence on derivatives in the z-direction, resulting in a system of ordinary differential equations. Also, we mandate that the enthalpies of formation are defined for the ambient temperature, so $T_\infty = T_0$. Generally, these enthalpies are available at 298 K, which is typical of room temperature. Furthermore, we dispense with the summation notation and allow

$$\sum h_{f,j}^0 \dot{m}_j''' = \Delta h_c \dot{m}_F'''. \tag{3.11}$$

From this point on, we parallel an analysis from Quintiere [29]; however, the reference analysis was developed for a one-dimensional vaporization process in rectilinear coordinates reminiscent of the Stefan problem [34]. For more concise nota-

tion, we also introduce $\theta_T = T - T_\infty$ and $\theta_F = Y_F - Y_{F,\infty}$. By incorporation of the assumptions and notation above, we may now write the conservation equations as

$$-r\Delta h_c \dot{m}'''_F = \frac{d}{dr}\left(r\rho v c_p \theta_T\right) - \frac{d}{dr}\left(r\rho\mathcal{D}\frac{d}{dr}\left(c_p\theta_T\right)\right) \tag{3.12}$$

$$r\dot{m}'''_F = \frac{d}{dr}\left(r\rho v \theta_F\right) - \frac{d}{dr}\left(r\rho\mathcal{D}\frac{d\theta_F}{dr}\right) \tag{3.13}$$

where the species conservation equation has been written for the "fuel species." Noting the obvious similarity between Eqs. 3.12 and 3.13, we multiply Eq. 3.13 by Δh_c and add the product to Eq. 3.12 to obtain the homogenous ordinary differential equation,

$$\frac{d}{dr}\left(r\rho v\left(c_p\theta_T + \Delta h_c\theta_F\right)\right) - \frac{d}{dr}\left(r\rho\mathcal{D}\frac{d}{dr}\left(c_p\theta_T + \Delta h_c\theta_F\right)\right) = 0. \tag{3.14}$$

Next, we will specify the boundary conditions for this ODE by using a stagnant film model. Far from the wick surface (more precisely, at the boundary layer interface), we have ambient conditions, namely, $Y_F = Y_{F,\infty}$ and $T = T_\infty$, so $\theta_T = \theta_F = 0$. A mass balance at the surface of the wick demands that the amount of mass passing through the wick in the condensed phase is equal to the sum of the amount leaving due to diffusion and bulk velocity transport as a vapor. This can be expressed as

$$\dot{m}'_{\text{condensed}} = \dot{m}'_{\text{vapor}} + \dot{m}'_{\text{diffusion}}. \tag{3.15}$$

The bulk mass flow rate through the surface of the wick is equal on the inside and

outside infinitesimal volumes and will be denoted $\dot{m}'_r$. Thus, we can state that $\dot{m}'_{\text{condensed}} = \dot{m}'_r Y_{F,l}$ where $Y_{F,l}$ is the mass fraction of fuel in the liquid (taken as unity) and $\dot{m}'_{\text{vapor}} = \dot{m}'_r Y_F(R)$. Additionally, we can express the mass flow due to diffusion as $\dot{m}'_{\text{diffusion}} = -2\pi r \mathcal{D} \frac{dY_F}{dr}$ evaluated at $r = R$. Therefore, the boundary condition imposed at the wick surface is

$$\dot{m}'_F Y_{F,l} = \dot{m}'_F Y_F(R) - 2\pi R \rho \mathcal{D} \frac{dY_F}{dr}\Big|_{r=R}, \tag{3.16}$$

where $\dot{m}'_r = \dot{m}'_F$ because $Y_F = 1$ within the wick (the term $Y_F(R)$ is retained for clarity in subsequent analysis).

A similar argument is made to determine the heat transfer boundary condition at the wick surface. We know that the rate of energy loss due to fluid transport through the wick surface must balance that of conduction inwards from the fluid because no increase in temperature is possible with the liquid at its boiling point. This enables us to balance heat as

$$0 = \frac{\dot{m}'_F H}{c_p} - 2\pi R \frac{k}{c_p} \frac{dT}{dr}\Big|_{r=R}. \tag{3.17}$$

Above, the quantity H represents the heat of gasification adjusted to T_∞, which includes the enthalpy of solid-solid phase changes, enthalpy of fusion (solid-liquid), heating from melting temperature to vaporization temperature, and enthalpy of vaporization (liquid-vapor). By again invoking the unity Lewis number assumption

and multiplying the equation above by c_p,

$$0 = \dot{m}'_F H - 2\pi R c_p \rho \mathcal{D} \frac{dT}{dr}\Big|_{r=R}. \tag{3.18}$$

Again noting a similarity, we multiply Eq. 3.16 by Δh_c and add the product to Eq. 3.18 to obtain

$$0 = \dot{m}'_F \left(H + \Delta h_c \left(Y_F(R) - Y_{F,l}\right)\right) - 2\pi R \rho \mathcal{D} \left(c_p \frac{dT}{dr} + \Delta h_c \frac{dY_F}{dr}\right). \tag{3.19}$$

At this point, it is expedient to introduce β and ψ,

$$\beta = c_p \theta_T + \Delta h_c \theta_F \qquad \psi = 2\pi\rho\mathcal{D} = 2\pi k/c_p \tag{3.20}$$

so that the governing equation, Eq. 3.14, and its boundary conditions can be rewritten in the succinct form

$$\dot{m}'_F \frac{d\beta}{dr} - \psi \frac{d}{dr}\left(r \frac{d\beta}{dr}\right) = 0 \tag{3.21}$$

$$\begin{aligned} r = R: &\quad 0 = \dot{m}'_F \left(H + \Delta h_c \left(Y_F(R) - Y_{F,l}\right)\right) - R\psi \tfrac{d\beta}{dr} \\ r = \delta: &\quad \beta = 0 \end{aligned} \tag{3.22}$$

where use has been made of the fact $2\pi r \rho v(r) = Y_{F,l}\dot{m}'_r = \dot{m}'_F$ is independent of r for a nonreacting flow. Although these equations are more compact than their predecessors, we are able to move a step further by nondimensionalizing β as

$$\beta^* = \frac{\beta}{H + \Delta h_c \left(Y_F(R) - Y_{F,l}\right)}. \tag{3.23}$$

The resulting equation and boundary conditions are as follows:

$$\dot{m}'_F \frac{d\beta^*}{dr} - \psi \frac{d}{dr}\left(r \frac{d\beta^*}{dr}\right) = 0 \tag{3.24}$$

$$\begin{aligned} r = R: &\quad \tfrac{d\beta^*}{dr} = \tfrac{1}{R}\tfrac{\dot{m}'_F}{\psi} \\ r = \delta: &\quad \beta^* = 0. \end{aligned} \tag{3.25}$$

The problem specified by Eqs. 3.24 and 3.25 is well-posed and has the analytical solution

$$\beta^*(r) = \left(r^\lambda - \delta^\lambda\right) R^{-\lambda} \tag{3.26}$$

where $\lambda = \dot{m}'_F/\psi$. In Eq. 3.26, β^* is the dependent variable, r is the independent variable, and both R and δ are constants presumed to be known. The dimensionless vaporization rate, λ, however, is an eigenvalue of this equation. By solving for β^* at $r = R$, we obtain

$$\beta^*(R) = 1 - \left(\frac{\delta}{R}\right)^\lambda, \tag{3.27}$$

which can be manipulated to produce the vaporization rate,

$$\frac{\dot{m}'_F}{\psi} = \frac{\ln\left(1 - \beta^*(R)\right)}{\ln\left(\delta/R\right)}. \tag{3.28}$$

This equation can be rewritten in a more familiar form by starting with a different form of the conserved scalar, β^*. This is accomplished by considering Eq. 3.10 from the perspective of the oxidizer species rather than the fuel species and following a

similar analysis. This results in

$$\beta^*_{\mathrm{Ox}} = \frac{c_p\left(T - T_\infty\right) + \left(Y_{\mathrm{Ox}} - Y_{\mathrm{Ox},\infty}\right)\left(\Delta h_c/s\right)}{H}, \tag{3.29}$$

which can be substituted into Eq. 3.28 as

$$-\beta^*(R) = \frac{Y_{\mathrm{Ox},\infty}\left(\Delta h_c/s\right) - c_p\left(T_v - T_\infty\right)}{H} \equiv B. \tag{3.30}$$

where $Y_{\mathrm{Ox}}(R) = 0$ and H can be found in Table 3.1. Equation 3.30 defines the Spalding B number. The numerator can be viewed as the net energy released per unit mass of fuel consumed whereas the denominator is a measure of the amount of energy needed to vaporize that unit mass of fuel. Finally, we rewrite Eq. 3.28 in terms of k/c_p as

$$\frac{\dot{m}'_F(z)c_p}{k} = 2\pi\frac{\ln\left(1+B\right)}{\ln\left(\delta/R\right)}, \tag{3.31}$$

which is equivalent to the result obtained by Pagni [17].

To proceed, we approximate the boundary layer as a conducting annular shell (the "shell approximation") surrounding the wick. It can be shown [35] that the relationship between boundary layer thickness from a heated, vertical cylindrical surface to the Nusselt number of the flow may be expressed as $\mathrm{Nu}_{D,z} = 2/\ln\left(\delta/R\right)$. By substitution into Eq. 3.31, we can relate the mass transfer process to convection as

$$\frac{\dot{m}'_F(z)c_p}{k} = \pi\ln\left(1+B\right)\mathrm{Nu}_{D,z}(z) \tag{3.32}$$

A correlation exists that approximates the local Nusselt number [36] along the wick in the vertical direction,

$$\frac{\mathrm{Nu}_{D,z}}{\mathrm{Gr}_z^{1/4}} = 0.24\,\frac{z}{R}\left[\frac{\mathrm{Gr}_z}{4}\right]^{-1/4} + 0.40\,\mathrm{Pr}^{3/10}, \tag{3.33}$$

which can be expressed as

$$\mathrm{Nu}_{D,z} = 0.68 + 0.40\,\mathrm{Pr}^{1/20}\left(\mathrm{Ra}_D D/z\right)^{1/4}. \tag{3.34}$$

This correlation is accurate within 5% for $\mathrm{Ra}_D D/L = 2^{10}\,\mathrm{Pr}/\xi^4$ for $0 \leq \xi \leq 10$, or $\mathrm{Ra}_D D/L \geq 0.074$ [36]. Also, the heat transfer over the full length of the wick can be integrated using Eq. 3.34 to obtain the average Nusselt number for wick length as

$$\overline{\mathrm{Nu}}_{D,L} = 0.68 + 0.53\,\mathrm{Pr}^{1/20}\left(\mathrm{Ra}_D D/L\right)^{1/4}. \tag{3.35}$$

Similarly, it is possible to integrate Eq. 3.32 to obtain an expression for the total mass flow from the lateral region of the wick,

$$\frac{\dot{m}_{F,L} c_p}{kL} = \pi \ln\left(1+B\right)\overline{\mathrm{Nu}}_{D,L}. \tag{3.36}$$

Equations 3.34 and 3.35 both suggest a limiting Nusselt number of 0.68 as the wick becomes infinitely slender. Also, for gases, the term $\mathrm{Pr}^{1/20}$ is negligible as it holds a value of approximately 0.98.

3.3 Top Disc Mass Flow

One of the assumptions of this analysis was that the entire wick surface remains bathed in liquid fuel. One consequence of this assumption is that self-trimming wicks are excluded from this application for two reasons: first, such wicks are designed to desiccate at a desired length so that they may be trimmed by the flame; and second, such wicks also are made to burn in a bent shape, in contrast to the wicks that were intentionally kept as vertical as possible in these experiments. Another consequence of the bathed wick assumption is that the idealized disc surface atop the wick also releases fuel.

The mass flux from this surface is modeled as being driven by natural convection exclusively. However, this is a false condition because viscosity effects from the upward flow of fuel-products mixture from the wick sidewall will affect mass flux in the circular region. Nonetheless, this combined forced/free convection problem is treated as pure free convection.

As will be shown later, the range of Ra_D examined is approximately 10^{-3} to 10^6 and experimental data gathered for candles represents a range of approximately 0.1 to 50. One expression for the Nusselt number of a flow over a finite, horizontal hot plate in air for this range of Ra_D can be fitted to curves in Gebhart [37],

$$\overline{\mathrm{Nu}}_{D,D} = 0.43 + 0.6\,\mathrm{Ra}_D^{1/4}. \tag{3.37}$$

By making the approximation that the slope of the gas temperature curve at

the wick surface is approximately equal to the ratio of temperature difference to an abstract "boundary layer thickness" δ_t atop the disc and assuming that the saturated liquid fuel is present, one can write $h_c \approx k/\delta_t$ and obtain the approximate mass flux at the disc [29]

$$\dot{m}''_F \approx \frac{h_c}{c_p} \ln(1+B). \tag{3.38}$$

We can then multiply through by $\pi D^2/4$ and simplify to obtain the mass flow from the disc,

$$\dot{m}_{F,D} \approx \frac{\pi}{4} \frac{k}{c_p} D \ln(1+B) \, \overline{\mathrm{Nu}}_{D,D}, \tag{3.39}$$

or, in dimensionless form as

$$\frac{\dot{m}_{F,D} c_p}{kD} \approx \frac{\pi}{4} \ln(1+B) \, \overline{\mathrm{Nu}}_{D,D}. \tag{3.40}$$

3.4 Total Boundary Layer Mass Flow

In Eq. 3.3, we left ambiguous the profile of the axial velocity curve. To complete this analysis, however, we must specify one. We have selected to model the axial velocity as the zeroth-order expansion from LeFevre and Ede [32],

$$u(y,z) = C_0 \sqrt{z} \frac{y}{y_\delta} \left(1 - \frac{y}{y_\delta}\right)^2, \tag{3.41}$$

where

$$C_0 = \frac{80\alpha_m}{B_0^2} \qquad \text{and} \qquad B_0^4 = \frac{80}{21} \frac{(20 + 21\mathrm{Pr})\,\alpha_m^2}{g\mu_m\theta_1}. \tag{3.42}$$

In these expressions, material properties have again been calculated for the fuel-products mixture. The expression for B_0 reflects a correction made to the original source. Furthermore, while the term θ_1 reflects the temperature difference between the cylinder's surface and ambient air in a pure heat transfer model, the situation is more tenuous due to the temperature profile caused by the flame. Because the thrust of the idea is to model the buoyancy effects, we choose $\theta_1 = T_f - T_\infty$. Thus, we can simplify to

$$C_0 = 4\sqrt{\frac{105\, g\mu_m\,(T_f - T_\infty)}{20 + 21\mathrm{Pr}}}. \tag{3.43}$$

Variable C_0 has dimensions of $\mathrm{L}^{1/2}\ \mathrm{t}^{-1}$.

The parameterization in Eq. 3.41 has some correct qualitative behaviors, as shown in Fig. 3.3. For instance, the velocity becomes zero at the wick surface (no-slip condition) and also at the boundary layer edge, which is close to the 1% of ambient commonly taken as defining the boundary layer. Also, the curve rises quickly to a peak velocity before tapering off.

Equation 3.3 calls for the integral of $ru(r, z)$ with respect to r. To calculate this integral, we apply the transformation $r = y + R$ to Eq. 3.41 and evaluate at $z = L$ to obtain

$$\dot{m}(L) = \frac{\pi}{15} C_0 \rho_m \sqrt{L} D^2 \frac{y_\delta}{D}\left(\frac{5}{4} + \frac{y_\delta}{D}\right), \tag{3.44}$$

where an extra D/D factor has been introduced. Equation 3.44 now has the expected $\sqrt{L}$ scaling factor. By multiplying through by c_p/k (again evaluated at T_m), we can

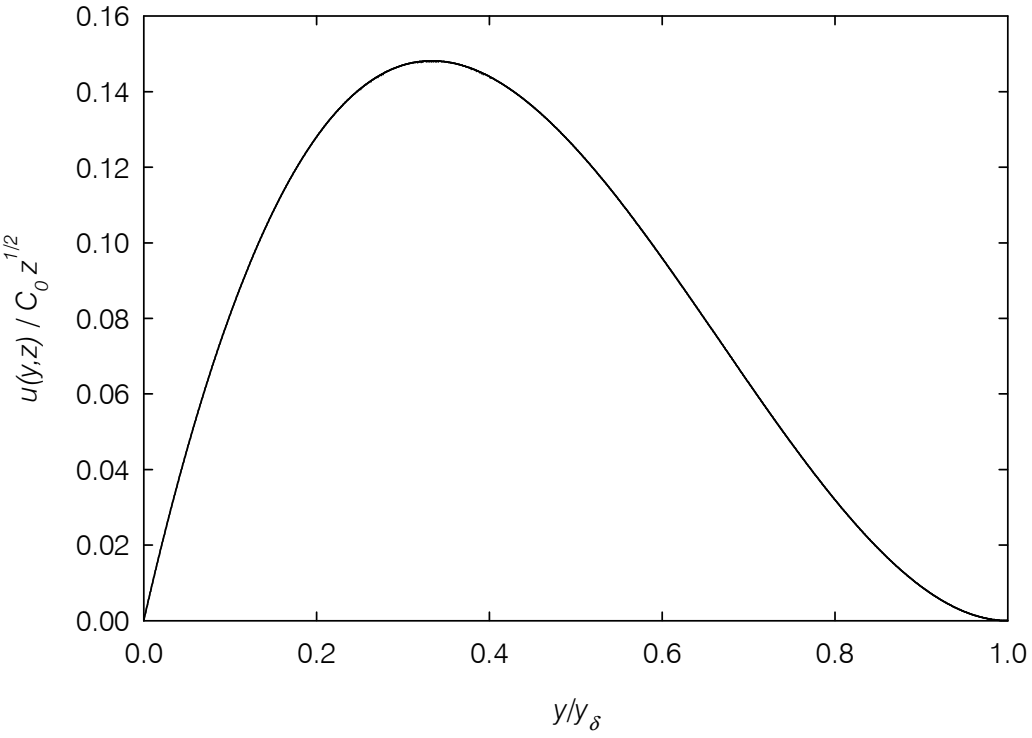

Figure 3.3: Boundary layer velocity profile curve for a slender vertical rod in natural convection [32].

express the total mass flow in nondimensional terms as

$$\frac{\dot{m}(L)c_p}{kL} = \frac{\pi}{15} C_0 \frac{\rho_m c_p}{k} \sqrt{L^3} \left[\frac{D}{L}\right]^2 \frac{y_\delta}{D} \left(\frac{5}{4} + \frac{y_\delta}{D}\right), \tag{3.45}$$

where an extra $\sqrt{L^2}/L$ factor has been introduced. Next, we substitute $\alpha_m = k/\rho_m c_p$ and C_0 from Eq. 3.43. After rearranging terms, we have

$$\frac{\dot{m}(L)c_p}{kL} = \frac{\pi}{15} \sqrt{\mathrm{Pr}} \left[\frac{4^2\, 105}{20 + 21\,\mathrm{Pr}}\right]^{1/2} \left[\frac{g\mu_m \left(T_f - T_\infty\right) D^3}{\alpha_m^2 \mathrm{Pr}} \frac{D}{L}\right]^{1/2} \frac{y_\delta}{D} \left(\frac{5}{4} + \frac{y_\delta}{D}\right). \tag{3.46}$$

Finally, we replace the first bracketed term in this equation with C_1 and the second with $\sqrt{\mathrm{Ra}_D D/L}$ to produce

$$\frac{\dot{m}(L)c_p}{kL} = \frac{\pi}{15} C_1 \sqrt{\mathrm{Pr}} \sqrt{\mathrm{Ra}_D D/L}\, \frac{y_\delta}{D} \left(\frac{5}{4} + \frac{y_\delta}{D} \right), \tag{3.47}$$

where C_1 is a velocity scaling factor and is calculated to have a value of 6.9 from an analytical approach. This factor is not known precisely and its interpretation is complicated by the presence of a flame sheet, which does not appear in the analogous pure convection scenario.

3.5 Boundary Layer Thickness and Flame Standoff Distance

The thickness of the boundary layer can be calculated by modeling the boundary layer as an annular shell around the wick, which transfers heat via conduction [35]. This thickness can be calculated from the Nusselt number by again invoking the shell approximation,

$$\mathrm{Nu}_{D,z} = \frac{2}{\ln\left(1 + y_\delta(z)/R\right)}, \tag{3.48}$$

and solving for y_δ to obtain the thermal boundary layer thickness,

$$y_\delta(z) = R\left(\exp\left(2/\mathrm{Nu}_{D,z}\right) - 1\right). \tag{3.49}$$

The position of the flame relative to the boundary layer can be calculated by extending the conserved scalar approach of Section 3.2, which has been taken from Quintiere [29]. We begin by realizing that because the original fuel atoms can neither

be created nor destroyed, we can define a mixture fraction f of fuel atoms that must obey the sourceless conservation equation

$$\dot{m}'_F \frac{df}{dr} - \psi \frac{d}{dr}\left(r \frac{df}{dr}\right) = 0, \tag{3.50}$$

with the boundary conditions

$$\begin{aligned} r = R: &\quad \dot{m}'_F Y_{F,l} = \dot{m}'_F f(R) - R\psi \frac{df}{dr}\Big|_{r=R}, \\ r = \delta: &\quad f = 0. \end{aligned} \tag{3.51}$$

The mixture fraction at the surface is denoted by $f(R)$ and has a boundary condition identical to Eq. 3.16, the boundary condition for the chemical fuel species. The mixture fraction at $r = \delta$ equals zero because fuel is assumed to come from the wick only (pure diffusion flame) and be consumed entirely in the flame sheet. As with β, we normalize f in accordance with its boundary conditions to obtain $f^* = f/\left(f(R) - Y_{F,l}\right)$. In so doing, the governing equation, Eq. 3.50, once rewritten for f^*, becomes identical to Eq. 3.21 and the boundary conditions become identical to Eq. 3.25. Because the governing equations and the boundary conditions are identical, uniqueness dictates that one solution exists and is common to both β^* and f^*. Thus,

$$\beta^* = f^* = \frac{f}{f(R) - Y_{F,l}}. \tag{3.52}$$

Equation 3.52 allows us to calculate the mixture fraction at the surface by eval-

uating the equation at $r = R$ to obtain

$$f(R) = \frac{\beta^*(R)\, Y_{F,l}}{\beta^*(R) - 1} = \frac{B\, Y_{F,l}}{1 + B}. \tag{3.53}$$

By choosing to express β^* in terms of the oxidizer and fuel species mass fractions, it can be shown [29] that the stoichiometric value of mixture fraction, f_f, is

$$f_f = (Y_{\mathrm{Ox},\infty}/s) \Big/ \left(\frac{Y_{\mathrm{Ox},\infty}}{s Y_{F,l}} + 1 \right). \tag{3.54}$$

This value of mixture fraction defines the position of the flame sheet, or $f_f = f(r_f)$. Equation 3.26 can be solved for r_f using $\beta^* = f^*$ to obtain $r_f^\lambda = \delta^\lambda + R^\lambda f_f^*$. Next, we can substitute Eq. 3.54 into Eq. 3.52 to obtain the stoichiometric value of f_f^* to produce the position of the flame sheet in radial coordinates,

$$r_f^\lambda = \delta^\lambda - R^\lambda \frac{Y_{F,l}\, Y_{\mathrm{Ox},\infty}}{(Y_{F,l} - f(R))\,(s Y_{F,l} + Y_{\mathrm{Ox},\infty})}. \tag{3.55}$$

The negative sign comes from inverting the order of terms in the denominator of Eq. 3.52. In a sense, Eq. 3.55 states that position of the flame front is a deduction from the position of the boundary layer, which is based on the radius of the wick and chemistry conditions.

Although the expression for r_f given by Eq. 3.55 expresses the quantity desired, it does so in terms of the unknowns δ and λ. To eliminate these variables, we divide

Eq. 3.55 by R^{λ} and simplify to obtain

$$\frac{r_f}{R} = \left[\left(\frac{\delta}{R} \right)^{\lambda} - \frac{Y_{F,l}\, Y_{\mathrm{Ox},\infty}}{(Y_{F,l} - f(R))\,(sY_{F,l} + Y_{\mathrm{Ox},\infty})} \right]^{1/\lambda}. \tag{3.56}$$

We continue by rewriting the fractional term (equal to $-\beta_f^*$) in more familiar terms by utilizing Eqs. 3.52–3.54 to obtain

$$\beta_f^* = -\frac{1+B}{1 + sY_{F,l}/Y_{\mathrm{Ox},\infty}}. \tag{3.57}$$

By expressing Eq. 3.31 in terms of λ as $\lambda = \ln(1+B) \,/\, \ln(\delta/R)$, we can rewrite Eq. 3.56 as

$$\frac{r_f}{R} = \left[1 + B - \frac{1+B}{1 + sY_{F,l}/Y_{\mathrm{Ox},\infty}} \right]^{1/\lambda}. \tag{3.58}$$

Equation 3.58 can be simplified further into the compact form

$$\frac{r_f}{R} = \left[\frac{1+B}{1 + Y_{\mathrm{Ox},\infty}/sY_{F,l}} \right]^{1/\lambda}. \tag{3.59}$$

Next, we invoke the shell approximation from Eq. 3.48 to substitute for λ, thereby coupling mass and heat transfer via the dimensionless group,

$$\lambda = \frac{1}{2}\mathrm{Nu}_{D,z} \ln(1+B). \tag{3.60}$$

This allows us to write

$$\frac{r_f}{R} = \frac{w}{D} = \left[\frac{1+B}{1+Y_{\mathrm{Ox},\infty}/sY_{F,l}}\right]^{2/\mathrm{Nu}_{D,L}\ln(1+B)}, \tag{3.61}$$

where Eq. 3.61 has been expressed at $z = L$. Equation 3.61 can be written in terms of the stoichiometric mixture fraction via Eq. 3.54 as

$$\frac{r_f}{R} = \frac{w}{D} = \left[\frac{1+B}{Y_{\mathrm{Ox},\infty}/sf_f}\right]^{2/\mathrm{Nu}_{D,L}\ln(1+B)}. \tag{3.62}$$

It is possible to separate the chemistry terms from the fluid mechanical terms by writing Eq. 3.61 as

$$\frac{r_f}{R} = \frac{w}{D} = \left[\left(\frac{1+B}{1+Y_{\mathrm{Ox},\infty}/sY_{F,l}}\right)^{1/\ln(1+B)}\right]^{2/\mathrm{Nu}_{D,L}}, \tag{3.63}$$

where the chemistry-driven terms are denoted by parentheses and the fluid mechanical terms by the square brackets.

Yet another form of Eq. 3.63 is possible: we can express y_f/y_δ, or the ratio between flame position and boundary layer thickness. By substituting $r_f = R + y_f$ and employing Eq. 3.49 for the boundary layer thickness, $\delta = R + y_\delta$, the resulting relationship is

$$\frac{y_f}{y_\delta} = \frac{\left[\frac{1+B}{1+Y_{\mathrm{Ox},\infty}/sY_{F,l}}\right]^{2/\mathrm{Nu}_{D,L}\ln(1+B)} - 1}{\exp\left(2/\mathrm{Nu}_{D,L}\right) - 1}. \tag{3.64}$$

3.6 Overwick Flame Height

The final task to calculate the gross dimensions of a candle flame is to determine the height of the flame above the wick. As previously mentioned, all experimental cases produced flame heights that extended beyond the wick tip, even those with narrow diameters. This allows us to conclude that the fuel combusted over the wick largely originates from the wick sides. Furthermore, it was observed that the maximum flame diameter coincides with the tip of the wick; therefore, we consider the horizontal circular regions formed by the flame. This region will be modeled as a circular port burner with the flow rate of fuel prescribed by Eq. 3.8.

A well-respected body of literature on the subject of gaseous port burners exists due to Roper [1, 38]. In particular, these sources provide expressions of the length of the flame in the overwick region (where the volumetric flow rate has been adjusted to ambient temperature) based on theory as

$$L_f = \frac{1}{4\pi} \frac{\dot{V}_F(T_\infty)}{\ln\left(1 + 1/S\right)} \frac{\left(T_\infty/T_f\right)^{2/3}}{\mathcal{D}_\infty} \tag{3.65}$$

and one adjusted based on experimental observations with gaseous fuels as

$$L_f = \left(1330 \, \frac{\mathrm{s}}{\mathrm{m}^2}\right) \frac{\dot{V}_F(T_\infty)}{\ln\left(1 + 1/S\right)}, \tag{3.66}$$

in which S is the molar stoichiometric air-fuel ratio.

The measurements given by Eq. 3.66 and those experimentally measured in a similar fashion generally pertain to flames exhibiting yellow luminosity from soot.

In contrast, this analysis considers the width and length of stoichiometric regions. For yellow flames, the stoichiometric and luminous widths are nearly the same. However, the luminous lengths are typically twice as long as stoichiometric, as shown in Sunderland et al. [39].

Application of Eqs. 3.65 and 3.66 is problematic because they are expressed for gaseous fuels with a uniform fluid temperature at the burner mouth. A secondary issue is that Roper's [1] formulation considers the volumetric flow rate of fuel whereas analysis of candle flames is more naturally expressed in mass flow rate; therefore, an approximate average fuel density is required to marry the approaches.

In the candle flame, the "apparent port burner" coincides with the plane of the flame at its widest diameter and actually has a temperature profile where the temperature is equal to vaporization temperature, T_v, for $0 \leq r \leq R$ and then increases to T_f at $r = r_f$. However, in keeping with the original model, we shall model the gaseous fuel at its vaporization temperature, T_v. Using a constant temperature, an estimate of the mass density of the fuel can be identified. To express Roper's [1] theory from the perspective of mass flow rate rather than volumetric, we begin with his equation,

$$\Theta = \frac{4\mathcal{D}_f z T_v}{w^2 u T_f}, \tag{3.67}$$

where the diffusivity has been taken at the flame temperature because the narrow zone near the flame sheet in which concentration gradients are steep dominates the diffusion process. Similarly, Eq. 3.65 adjusts $\mathcal{D}$ to the flame temperature with the

approximation $\mathcal{D}(T) = \mathcal{D}_{\text{ref}} \left(T/T_{\text{ref}}\right)^{5/3}$. Furthermore, Roper shows that

$$1 - \exp\left(-1/4\Theta\right) = \left(1 + S\right)^{-1} \tag{3.68}$$

when $z = L_f$. If we assume a uniform axial velocity, u, and $\dot{m}_F = \frac{1}{4}\pi w^2 u_1 \rho_v$, then Eq. 3.67 can be substituted into Eq. 3.68 and rearranged to obtain

$$L_f = \frac{T_f}{T_v} \frac{\dot{m}_F}{\rho_v \mathcal{D}_f} \frac{1}{4\pi \ln\left(1 + 1/S\right)}. \tag{3.69}$$

Recalling that $k/c_p = \rho\mathcal{D}$ is to be evaluated at T_m, we must adjust both the density and diffusivity of the above equation to this temperature. Because the molecular weight of the vaporized fuel is greatly different than the surrounding air, we must consider its effect via the ideal gas law,

$$\frac{\rho_m}{\rho_v} \approx \frac{M_\infty T_v}{M_F T_m}. \tag{3.70}$$

After substituting Eq. 3.70 into Eq. 3.69 and adjusting the diffusivity to $\mathcal{D}_m$, we may divide through by L to obtain

$$\frac{L_f}{L} = \frac{\dot{m}_F c_p}{kL} \frac{M_\infty}{M_F} \left[\frac{T_m}{T_f}\right]^{2/3} \frac{1}{4\pi \ln\left(1 + 1/S\right)}. \tag{3.71}$$

Finally, we apply the definition $T_m = \left(T_f + T_v\right)/2$ and simplify to obtain

$$\frac{L_f}{L} = \frac{\dot{m}_F c_p}{kL} \frac{M_\infty}{M_F} \left[1 + \frac{T_v}{T_f}\right]^{2/3} \frac{1}{4^{4/3}\pi \ln\left(1 + 1/S\right)}. \tag{3.72}$$

It can be shown [33] for a hydrocarbon fuel with a composition C_xH_y that S is

$$S = \frac{x + y/4}{X_{O_2}}, \tag{3.73}$$

where X_{O_2} is the mole fraction of oxygen in air and has a value of approximately 21%. Paraffin is composed primarily of high molecular weight alkanes, which have the general form C_nH_{2n+2} where $22 \leq n \leq 27$ and participates in the general combustion reaction (in air)

$$C_nH_{2n+2} + \left(\frac{3}{2}n + \frac{1}{2}\right)\left(O_2 + \frac{1 - X_{O_2}}{X_{O_2}}N_2\right) \rightarrow$$
$$nCO_2 + (n+1)\,H_2O + \frac{1 - X_{O_2}}{X_{O_2}}\left(\frac{3}{2}n + \frac{1}{2}\right)N_2. \tag{3.74}$$

We can rewrite S in terms of n or s as

$$S = \frac{3n+1}{2X_{O_2}} = \frac{M_F}{M_\infty}\frac{s}{Y_{Ox,\infty}}. \tag{3.75}$$

Calculated values of S and s are listed in Table 3.1 for straight-chain alkanes of weights typical to paraffin waxes. For this analysis, we arbitrarily select $n = 24$ (tetracosane) to represent the wax used in our candle experiments.

n	Chemical name	M_F (g/mol)	S (mol/mol)	s (kg/kg)	H (kJ/kg)
22	n-Docosane	310.60	159.52	3.45	620.7
23	n-Tricosane	324.63	166.67	3.45	603.5
24	n-Tetracosane	338.65	173.81	3.45	621.0
25	n-Pentacosane	352.68	180.95	3.45	592.6
26	n-Hexacosane	366.71	188.10	3.45	634.0
27	n-Heptacosane	380.73	195.24	3.45	615.9

Table 3.1: Names and properties of unbranched alkanes. H assumes an initial temperature of 298.15 K and is based on Chickos and Wilson [40]. ($X_{O_2} = 0.21, Y_{O_2} = 0.233, M_\infty = 28.85$ g/mol)

Chapter 4

Results

In this chapter, the model of Chapter 3 is compared with flame length and width measurements for paraffin candles.

4.1 Fuel Vaporization Rates

The candle flame model presented offers two distinct regions of fuel supply: the lateral and horizontal (top) areas of the idealized cylindrical wick. For the top, Eq. 3.40 predicts the fuel vaporization rate and is plotted in Fig. 4.1. It is possible to rewrite Eq. 3.40 to include the dimensionless group $\mathrm{Ra}_D D/L$ and slenderness ratio D/L as

$$\frac{\dot{m}_{F,D} c_p}{kL} = \frac{\pi}{4} \ln(1+B) \left(0.43 \frac{D}{L} + 0.6 \left[\mathrm{Ra}_D \frac{D}{L} \right]^{1/4} \left[\frac{D}{L} \right]^{3/4} \right). \tag{4.1}$$

The wick top fuel supply rate is plotted along these axes in Fig. 4.2.

For the sides of the wick, the fuel vaporization rate is presented in Eq. 3.36 and is plotted in Fig. 4.3.

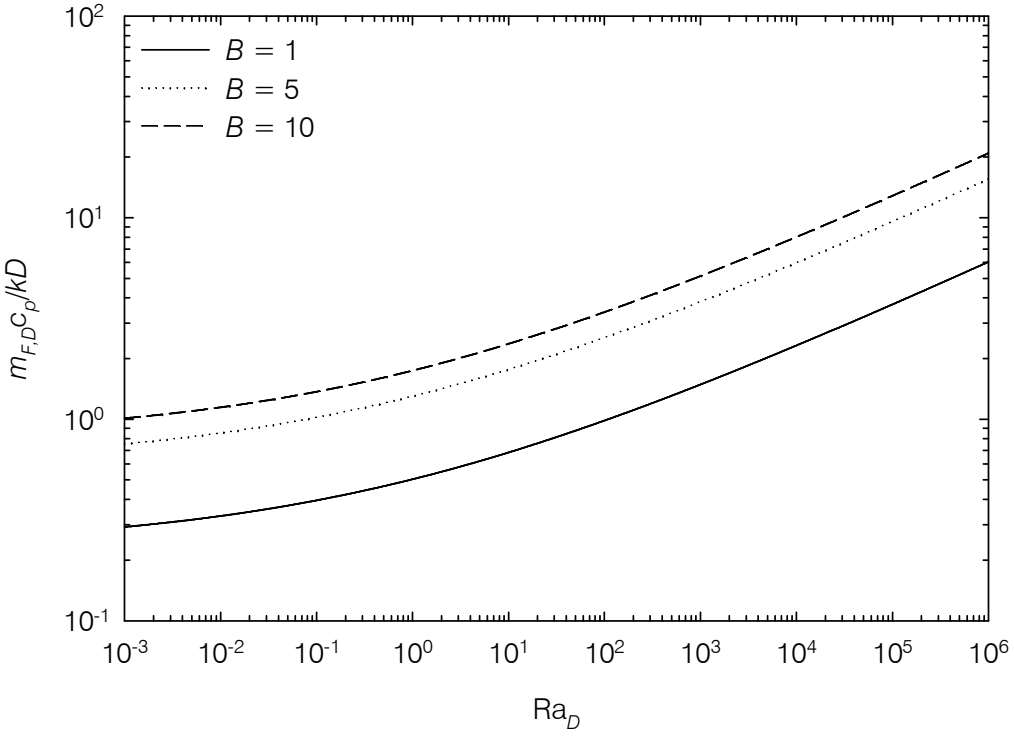

Figure 4.1: Wick top fuel vaporization rate $\dot{m}_{F,D}c_p/kD$.

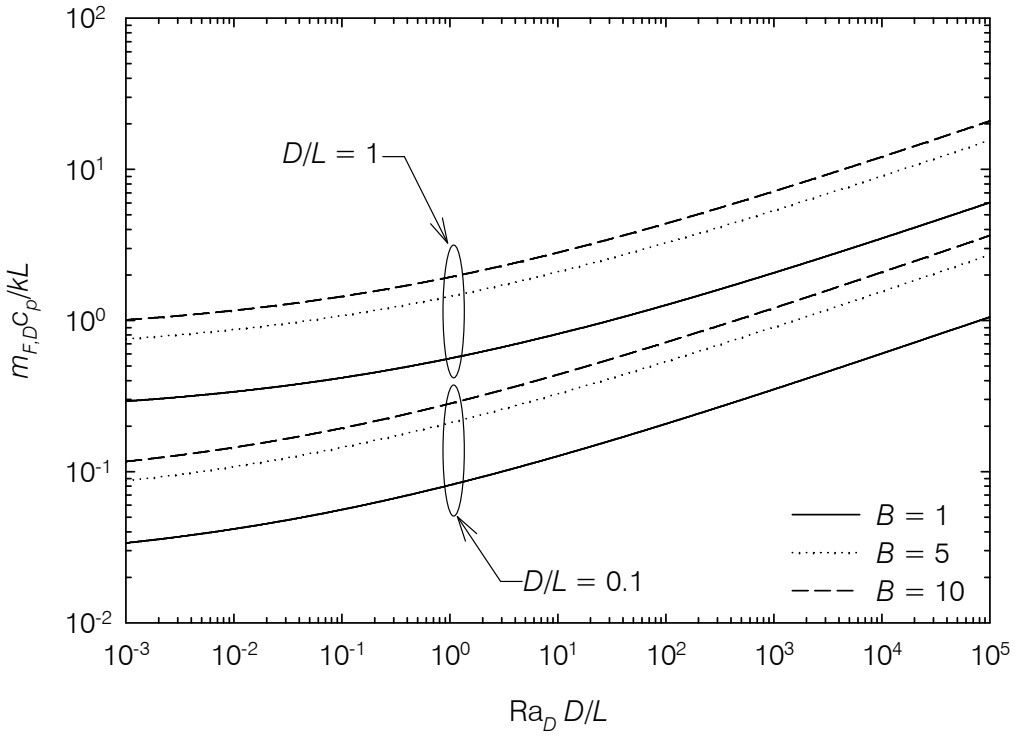

Figure 4.2: Wick top fuel vaporization rate expressed as $\dot{m}_{F,D}c_p/kL$ for comparison with the lateral fuel vaporization rate.

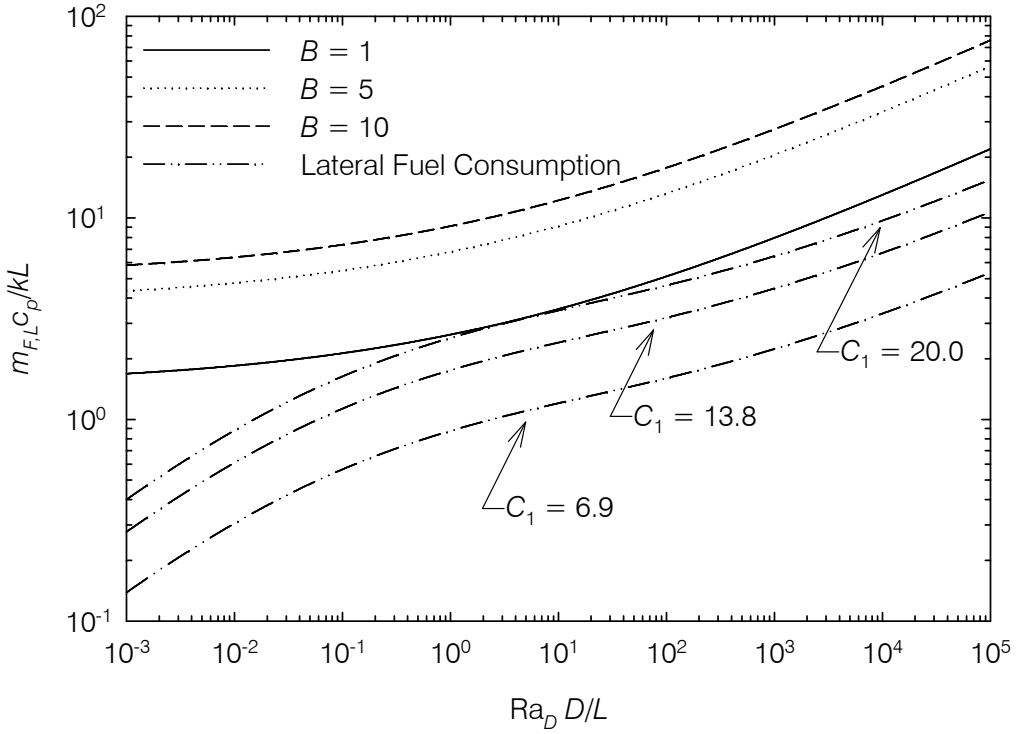

Figure 4.3: Wick lateral fuel vaporization rate $\dot{m}_{F,L}c_p/kL$ and lateral fuel consumption rate. (For constants, see Appendix C).

4.2 Flame Width

By modeling a candle flame as residing within the boundary layer of a stagnant, free-convective flow, we were able to obtain an expression (Eq. 3.63) for the position of the flame front at the interface between the lateral and overwick regions,

$$\frac{r_f}{R} = \frac{w}{D} = \left[\frac{1+B}{1+Y_{Ox,\infty}/sY_{F,l}}\right]^{2/\mathrm{Nu}_{D,L}\ln(1+B)}.$$

This expression implicitly defines the position of the maximum flame standoff distance to be at the interface mentioned above. This is necessary for the model because the region above the sidewall is modeled as a gaseous port burner with an unknown flame profile. However, this approximation is also a reasonable one because, in general, the majority of fuel supplied to the flame is supplied through the wick sides and therefore a near-maximum quantity of fuel has already been contributed by this position. Further, experimental evidence shows that the flame does indeed bulge only slightly above this location.

Equation 3.63 shows that there are several phenomena in play.

First, the position of the flame is normalized by the radius of the wick, rather than its length. The lack of a similar term on the right hand side of the equation is significant because this reveals that R (or D) is the dominant geometric factor in determining the position of the flame front. However, in this application, it is incorrect to state that wick length plays no role because $\mathrm{Nu}_{D,L}$, which is evaluated at $z = L$, is dependent upon L via correlation. This dependence manifests itself

physically as representing the length of the surface that provides the majority of fuel. Equation 3.63 predicts larger wick radii produce larger flames, as is expected.

Second, the Spalding B number plays a prominent role as the numerator of the exponent term and as part of the exponent itself. Recalling that larger values of B represent a lower resistance to vaporization, the flame expands with increasing B. This can be best understood by considering the inverse situation: a *lower* B number requires that the flame resides closer to the wick so that more heat can be conducted into the wick surface to vaporize the more resistant fuel. A larger B number is then more tolerant of greater standoff distances (i.e., shallower temperature gradients); combined with the propensity of fuel to seek oxidizer, the flame extends to the more plentiful oxygen at farther distances. That is, for a flow penetrating a circular surface in the normal direction at a given speed, a larger radius results in a higher volumetric flow rate, which provides more oxygen. The actual quantitative effect of changes in B are small, as can be seen in Fig. 4.4. This figure also shows that B takes on greater significance for smaller Nusselt numbers due to diminished heat flow into the liquid phase.

Third, stoichiometry and fuel composition play a role in the fraction $Y_{Ox,\infty}/sY_{F,l}$. For tetracosane in air, this has a value of 0.0676. This fraction has a practical range of about 0.025–1.0. Here, the lower end of the range represents fuels requiring high amounts of oxidizer where the ambient oxygen mass fraction is on the threshold of quenching, or $Y_{Ox,\infty} \approx 0.1$ and $s \approx 4$. The high end represents fuels requiring low amounts of oxidizer in an oxygen-rich environment, or $Y_{Ox,\infty} = 1$ and $s \approx 1$. In both cases, it was assumed that pure fuels ($Y_{F,l} = 1$) were being burned. The net effect is

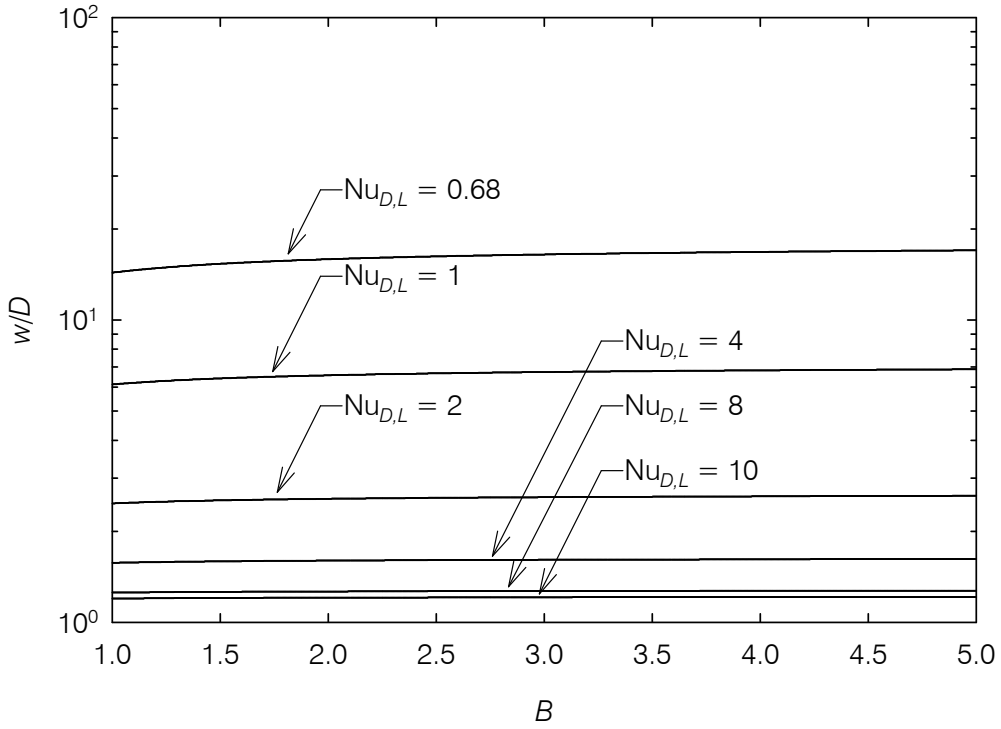

Figure 4.4: Sensitivity to w/D to changes in B. The range of $\mathrm{Nu}_{D,L}$ selected bounds the possible values calculated via Eq. 3.35 for $10^{-3} < \mathrm{Ra}_D D/L < 10^5$. ($Y_{Ox,\infty}/sY_{F,l} = 0.0676$).

that fuels under "easier" burning conditions (i.e., with higher values of the fraction) serve to decrease w/D. Numerically, this occurs because the inner denominator of Eq. 3.63 grows, causing the parenthesized term to decrease. Physically, this effect can be interpreted as similar to requiring less oxidizer, enabling the flame to dwell closer to the fuel surface.

Fourth, the greatest effect is given by the Nusselt number, which is a measure of the relative importance of convection to conduction heat transfer. There are two significant effects. First, larger values of $\mathrm{Nu}_{D,L}$ vaporize more fuel from the wick sides (though that effect is not visible in Eq. 3.63) and second, larger values of $\mathrm{Nu}_{D,L}$ result in higher flow velocities, which have the effect of sweeping the flame into a thinner profile. In this model, the second factor has a dramatic effect upon the flame width as can be seen in Fig. 4.5, which shows that for weakly convective scenarios ($\mathrm{Nu}_D < 1$), flames are expected to have wide breadths. Again, this is the manifestation of a conduction- (or mass diffusion-) dominated flame; in this sense, flames tend toward their behavior in microgravity [19]. Figure 4.5 also demonstrates the insensitivity of w/D to changes in B.

Comparison between observations and predictions require an intermediate calculation because $\mathrm{Nu}_{D,L}$ is not known *a priori.* To calculate $\mathrm{Nu}_{D,L}$, we can employ Eq. 3.34. Calculating $\mathrm{Nu}_{D,L}$ in this way, the flame width predicted is plotted as the solid curve in Fig. 4.6, where the abscissa has been replaced with the more basic variable, $\mathrm{Ra}_D D/L$. This figure shows that, on average, the observed flame width is about 52% as large as the predicted value. This is in line with Kosdon et al. [12], whose experimental flame standoff distance, y_f, was about half as large as

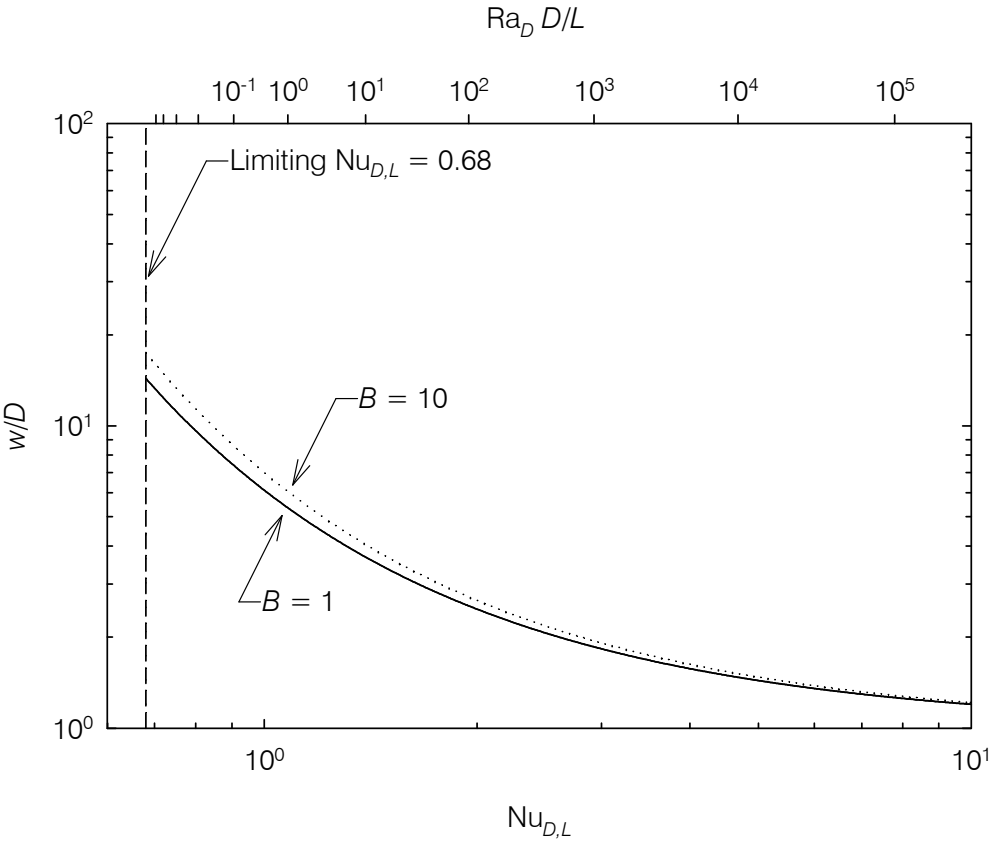

Figure 4.5: Sensitivity to w/D to changes in $\mathrm{Nu}_{D,L}$. ($Y_{Ox,\infty}/sY_{F,l} = 0.0676$)

that predicted by their theory. Also, the CFD results of Alsairafi [26], Raju [28] and Riley [24] are plotted for comparison. For consistency, material properties for tetracosane were substituted for any specified in the original reference to calculate the Rayleigh number as $\mathrm{Ra}_D/D^3 = 3.50 \times 10^8$ m^{-3}. In this way, all data points are directly comparable with results from this thesis.

Figure 4.6 shows qualitative agreement but quantitative disagreement. That is, the flame widths descend at the rate predicted with $\mathrm{Ra}_D D/L$ but the width itself is too high. As has been previously shown, w/D is not sensitive to choices of B and $Y_{\mathrm{Ox},\infty}/sY_{F,l}$ is constant for the possible hydrocarbon fuels; therefore, we must look elsewhere for the source of the error.

The most likely source of this discrepancy is that the shell approximation, Eq. 3.49, poorly approximates reality. This is excusable as the presence of the flame likely influences the position of the boundary layer. Furthermore, the existence of two colliding streams (fuel and oxidizer) creates radial velocities that are different from a cooling vertical cylinder undergoing natural convection. Unfortunately, multiplication of the right hand side of Eq. 3.60, which constitutes the reciprocal of the exponent in Eq. 3.61, does not result in the fit desired, suggesting a more complex relationship is required or that another source of error is involved.

One might suspect that experimental values of $\mathrm{Ra}_D D/L$ could be underpredicted, sliding the data points to the left in the plot. Classically, the Rayleigh number is defined by the temperature difference between the cylinder surface and ambient fluid. This is not representative of a cylinder surrounded by a flame, however, so instead the characteristic temperature difference was defined as that between the maximum

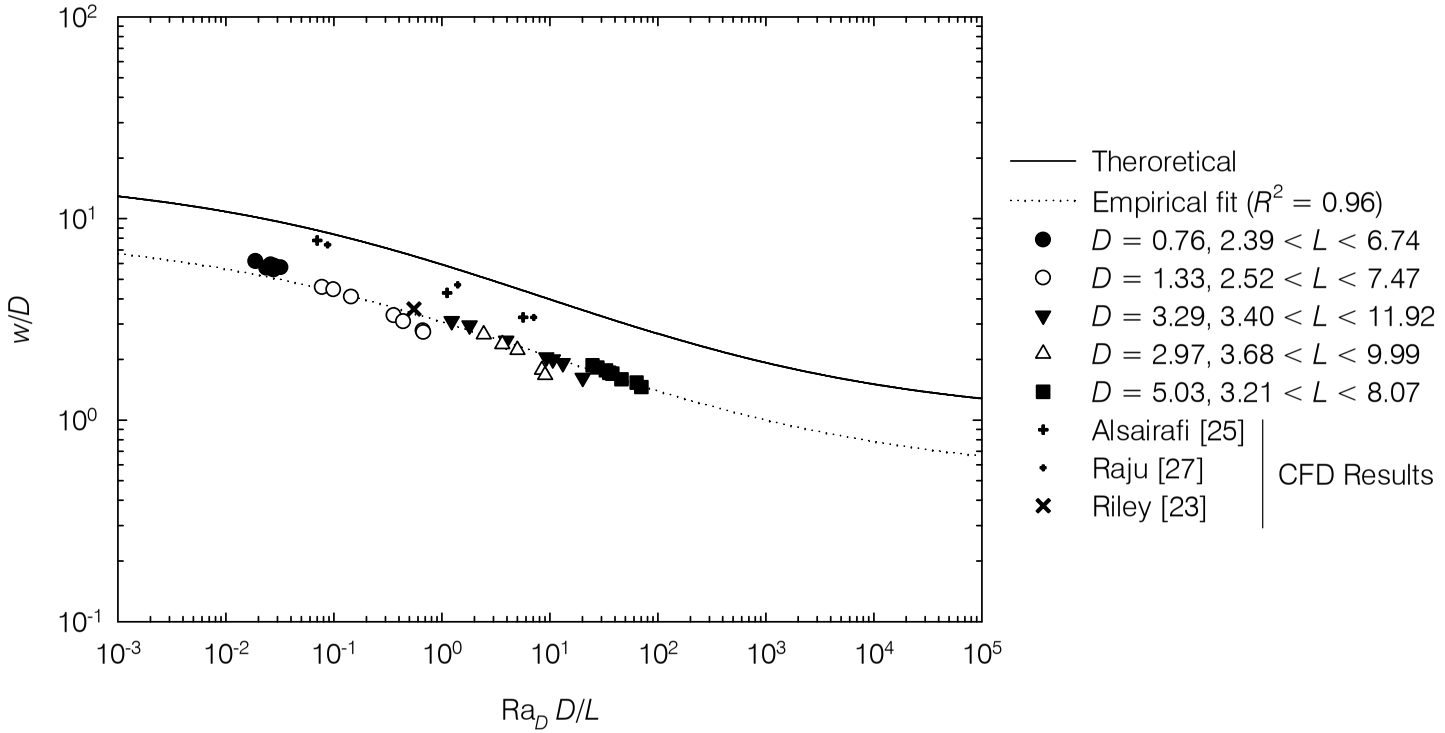

Figure 4.6: Observed and predicted w/D using an approximation for $\mathrm{Nu}_{D,L}$. Observed values of length, diameter and flame width were obtained via photometry. Diameter shown reflects the mean diameter for the samples tested and differs substantially from the unburnt wick. Units: mm. ($Y_{Ox,\infty}/sY_{F,l} = 0.0676, B = 4.29$; for other constants, see Appendix C).

flame temperature and the ambient gas. Any other choice of temperature difference would reduce Ra_D. The Rayleigh number can also be manipulated by alternate selections of α, Pr or μ_m. Of these, we know that the Prandtl number will not vary greatly. The expansion coefficient μ_m is defined as $1/T_m$; defining it as $1/T_f$ or $1/T_\infty$ would not change raise or lower Ra_D by more than a factor of 3, which is insufficient to shift the experimental data points to the right by the factor of 100 as is needed. Because Pr is approximately constant over a wide temperature range for most gases, ν is defined as $\alpha\mathrm{Pr}$, giving heavy weight to the choice of α. To translate the data points to the right as necessary for agreement with the curve, α must decrease by a factor of ten (because α^2 appears in the denominator of Ra). Such a departure from the nitrogen properties used is unlikely because the fuel-products mixture has a comparable molecular weight to nitrogen, the heavy fuel being among the minor species. Furthermore, an error in estimating thermal diffusivity would promulgate to the fuel vaporization rate due to the inclusion of k/c_p, the major component of the fuel mass flow nondimensionalizing group, within its definition.

Empirically, Eq. 3.63 can be adjusted by a constant factor of 0.52 to achieve a fit to data,

$$\frac{w_{\mathrm{emp}}}{D} = 0.52 \left[\frac{1+B}{1+Y_{Ox,\infty}/sY_{F,l}}\right]^{2/\mathrm{Nu}_{D,L}\ln(1+B)} . \tag{4.2}$$

This is plotted as the dotted line in Fig. 4.6.

4.3 Lateral Burning Rate and Boundary Layer Thickness

It is possible to express $\dot{m}'_F(z)$, the local burning rate per unit length of wick, in terms of the lateral vaporization rate by dividing Eq. 3.32 and 3.36 to obtain

$$\frac{L\,\dot{m}'_F(z)}{\dot{m}_{F,L}} = \frac{\mathrm{Nu}_{D,z}}{\overline{\mathrm{Nu}}_{D,L}}. \tag{4.3}$$

As is typical with boundary layer analyses, there is a singularity at $z = 0$ in the calculation of $\mathrm{Nu}_{D,z}$, which implies that the equation above fails near the leading edge of the boundary layer. If we limit our analysis to $z = L$, we can utilize flame width measurements that were taken nearby to approximate the lateral vaporization rate. This is necessary because burning rates were not measured and so direct comparison is not possible. However, it is possible to calculate the lateral vaporization rate from the flame width using Eq. 3.31 if a relationship between δ and w can be found. Previously, we employed the shell approximation to produce Eq. 3.64, which is an expression for y_f/y_δ. Fig. 4.7 shows that, for practical fuels, the flame lies near the edge of the boundary layer. That the flame lies close to the oxidizer is no surprise; this is reflected also in the small stoichiometric value of mixture fraction. In fact, in the limit of infinite air-fuel ratio, s, the "flame" coincides with the boundary layer.

Equation 3.32 suggests that $\dot{m}'_F \propto \mathrm{Nu}_{D,z}$, where $\mathrm{Nu}_{D,z}$ grows with $(\mathrm{Ra}_D D/z)^n$. The parameter in parentheses is proportional to $D^{4n}z^{-n}$; and therefore to $\dot{m}'_F \propto D^{4n}z^{-n}$. Temporarily setting aside the fact that n is a affixed a value of 0.25, this

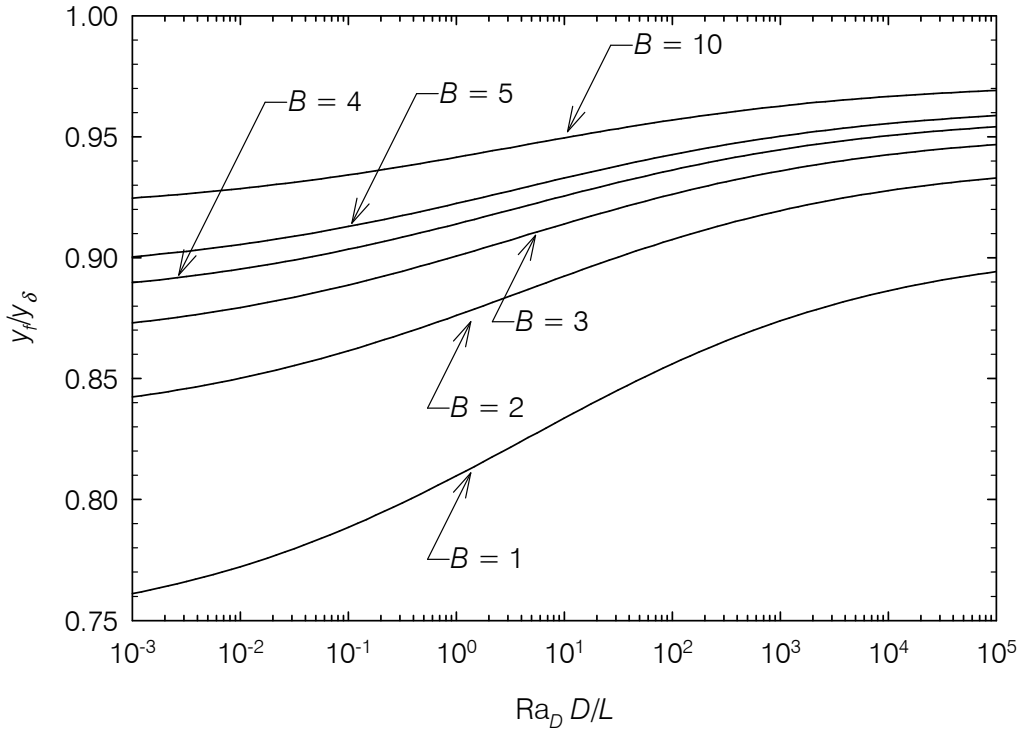

Figure 4.7: Relative position of the flame front, y_f/y_δ, using the shell approximation for $\mathrm{Nu}_{D,L}$. ($Y_{\mathrm{Ox},\infty}/sY_{F,l} = 0.0676$)

scaling law has some interesting properties.

First, it states that the fuel mass flux per unit length (g/s-m) decreases as one moves upwards along the wick; logically, this must be so because we prescribed an isothermal wick surface. Stated differently, a constant temperature differential between wick surface and ambient must have a decreasing mass flux because the flame grows in the radial direction, reducing the heat flux by decreasing the temperature gradient between the flame and wick surface. By contrast, the opposing case of a constant fuel mass flux boundary condition would require varying temperature or constant flame position. The latter case does not apply to the evaporative burning regime. This behavior is known in classical heat transfer literature.

Second, as expected, the mass flow increases with D. However, if we express the mass flux proper (i.e., mass flow per unit area) by dividing by πD, we find that $\dot{m}''_F \propto z^{-n_1} D^{4n_1-1}$. The significance of this scaling law is the transition to a flat-plate burning regime, i.e., for cylinders with large D/L ratios, flat plate behavior is anticipated. Indeed, the correlation employed to calculate $\mathrm{Nu}_{D,z}$ is based on the Nusselt number of a flat plate with a correction for curvature applied. Further, Nagendra [41] provides an exponent of $n = 0.25$ for "short cylinders/flat plates." Using the value of $n = 0.25$, we find that the dependence of $\dot{m}''_F$ on D vanishes. Additionally, the proportionality to $z^{-0.25}$ is also expected for a flat plate. Both of these facts are in agreement with flat plate theory.

The values for n have been discretized by correlation by Nagendra et al. [41] to include 0.05 for "wires" and 0.16 for "cylinders." However, physically, a continuous range is expected. Lyu and Chen [22] performed a numerical study of evaporation on

vertical porous cylinders in which they determined that the mass flux $\dot{m}''_F$ decreases with z and D. Although they do not supply exponents to fit into the Nagendra correlation, their results demonstrate that scaling law above has the correct qualitative behavior.

4.4 Total Burning Rate and Flame Length

The total mass flow rate of fuel being vaporized from the wick is the sum of the lateral and top component flow rates given by Eqs. 3.36 and 3.40,

$$\frac{\dot{m}_F c_p}{kL} = \pi \ln(1+B) \left(\frac{1}{4} \overline{\mathrm{Nu}}_{D,D} \frac{D}{L} + \overline{\mathrm{Nu}}_{D,L} \right), \tag{4.4}$$

where the dimensionless group $\mathrm{Nu} \ln(1+B)$ appears twice. This group contains a both a chemical term, $\ln(1+B)$, and convective-geometric term, Nu, which together give a measure of the fuel vaporization rate due to the presence of a flame in the surrounding stagnant layer.

The final property of the flame that we measure and model is the length of the flame. Both are based on straight wicks, whereas many consumer candles are of the self-trimming type in which the flame consumes the combustible wick by coming into contact with it. However, this description is slightly inaccurate because these typically slender wicks will curve somewhat and so the tip of the wick actually extends beyond the high point of the wick.

Nevertheless, the region of the flame above the wick is modeled as the circular port of a gaseous burner using the theoretical relationship from Roper [1] as the

basis and is presented as Eq. 3.72. Following from Eqs. 3.8, 3.47 and 4.4, we can consolidate an expression for the amount of fuel flowing from this imaginary burner as

$$\frac{\dot{m}_{F,b}c_p}{kL} = \pi \ln(1+B)\left(\frac{1}{4}\overline{\mathrm{Nu}}_{D,D}\frac{D}{L} + \left(1+\frac{Y_{\mathrm{Ox},\infty}}{s}\right)\overline{\mathrm{Nu}}_{D,L}\right) - \frac{Y_{\mathrm{Ox},\infty}}{s}\frac{\pi}{15}C_1\sqrt{\mathrm{Pr}}\sqrt{\mathrm{Ra}_D D/L}\,\frac{y_\delta}{D}\left(\frac{5}{4}+\frac{y_\delta}{D}\right), \quad (4.5)$$

where the second line of the equation is the lateral fuel consumption rate. Equation 4.5 is valid only for flames that extend above the wick. We rewrite Eq. 3.49 to include D rather than R and substitute for y_δ/D to produce

$$\frac{\dot{m}_{F,b}c_p}{kL} = \pi \ln(1+B)\left(\frac{1}{4}\overline{\mathrm{Nu}}_{D,D}\frac{D}{L} + \left(1+\frac{Y_{\mathrm{Ox},\infty}}{s}\right)\overline{\mathrm{Nu}}_{D,L}\right) - \frac{Y_{\mathrm{Ox},\infty}}{s}\frac{\pi}{60}C_1\sqrt{\mathrm{Pr}}\sqrt{\mathrm{Ra}_D D/L}\,\left(e^{2/\mathrm{Nu}_{D,L}}-1\right)\left(e^{2/\mathrm{Nu}_{D,L}}+\frac{3}{2}\right). \quad (4.6)$$

Equations 3.34, 3.35 and 3.37 can be substituted for $\mathrm{Nu}_{D,L}$, $\overline{\mathrm{Nu}}_{D,L}$ and $\overline{\mathrm{Nu}}_{D,D}$, respectively, to obtain the apparent circular port mass burning rate in terms of $\mathrm{Ra}_D D/L$. Finally, Eq. 4.6 can be substituted into Eq. 3.72 to calculate the dimensionless flame height above the wick,

$$\frac{L_f}{L} = \frac{\dot{m}_{F,b}c_p}{kL}\frac{M_\infty}{M_F}\left[1+\frac{T_v}{T_f}\right]^{2/3}\frac{1}{4^{4/3}\pi\ln(1+1/S)}. \quad (4.7)$$

This equation is plotted in Fig. 4.8 against flame measurements. The plot demonstrates qualitative agreement between theory and data. Also, the CFD results of

Alsairafi [26], Raju [28] and Riley [24] are plotted for comparison. For consistency, material properties for tetracosane were substituted for any specified in the original reference to calculate the Rayleigh number as $\mathrm{Ra}_D/D^3 = 3.50 \times 10^8$ m^{-3}. In this way, all data points are directly comparable with results from this thesis.

Candle flame lengths grow with increasing values of $\mathrm{Ra}_D D/L$, as expected, and at approximately the same rate as the data. Additional fuel is being vaporized commensurate with increased free-convection conditions. However, the quantitative disagreement of a factor of 2.7 too high on average implies that either the predicted fuel vaporization rate is too high, flame heights for a given amount of fuel are too high, the lateral fuel consumption rate is too low, or a combination of the above. Following the pattern of Eq. 3.66 (based on Roper [38]), an empirically-adjusted flame height equation can be expressed as

$$\frac{L_{f,\mathrm{emp.}}}{L} = 0.023 \, \frac{\dot{m}_{F,b} c_p}{kL} \frac{M_\infty}{M_F} \frac{1}{\ln\left(1 + 1/S\right)}, \tag{4.8}$$

in which a correction factor of 2.7 was applied, temperature terms have been folded into the numerical constant but the chemical terms have been retained explicitly. Also, the $4^{4/3}\pi$ term has been included within the constant. Inclusion of the temperature terms within the constant is believed to be appropriate as the value of $1 + T_v/T_f$ is not highly sensitive to the choice of fuel for paraffins. Equation 4.8 is plotted in Fig. 4.8 with the label "Fit."

The largest component of the discrepancy between Eq. 4.7 and data is likely due to the overprediction of fuel vaporization rates. In the absence of mass loss

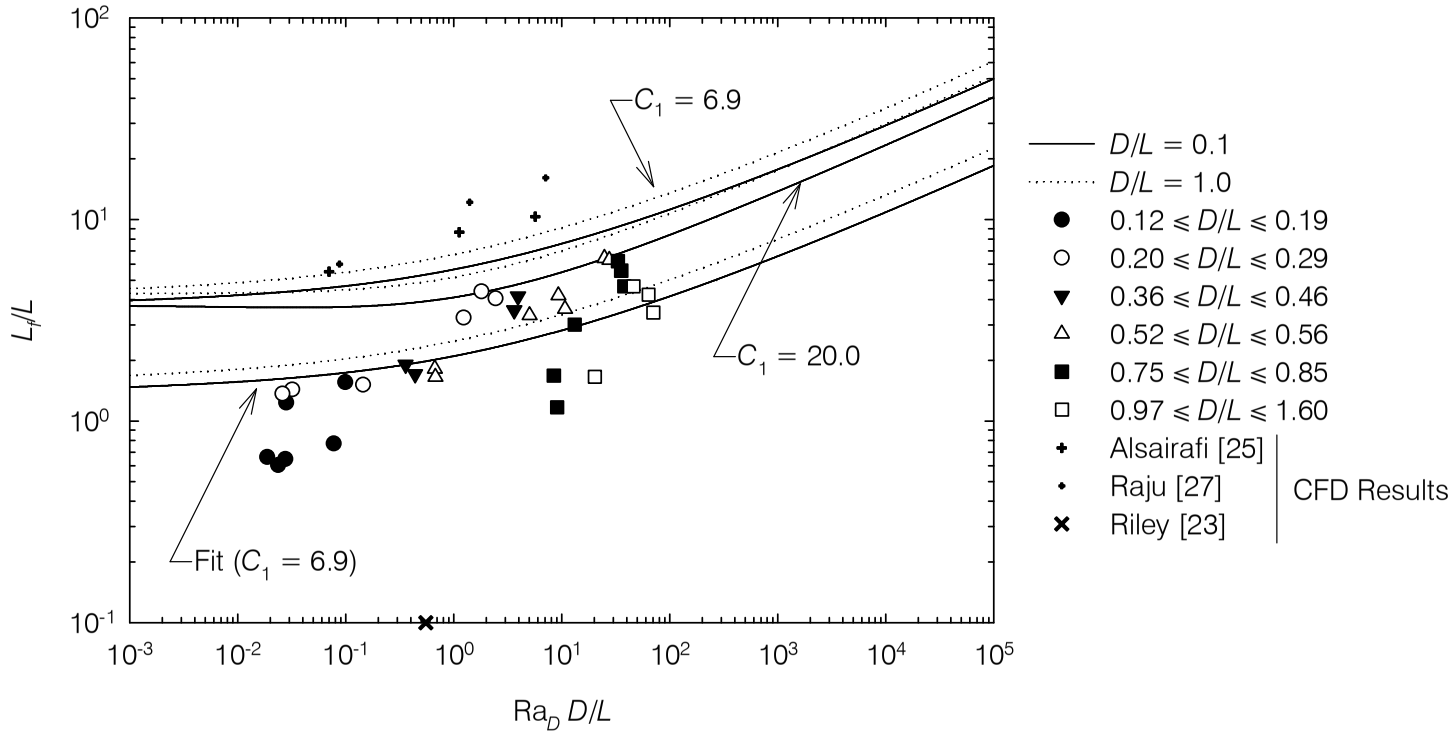

Figure 4.8: Flame height above the wick top, L_f/L. (For constants, see Appendix C).

measurements, we refer to the existing work of Hamins et al. [25] for corroboration with respect to mass loss rates. Steady state conditions for a *self-trimming* wick of diameter 1 mm and exposed length of approximately 12 mm embedded in a paraffin candle resulted in a mass burning rate of 0.105 g/min and overwick flame height of approximately 34 mm. In the dimensionless system used, these experimental data correspond to $\mathrm{Ra}_D D/L = 2.92 \times 10^{-2}$, $\dot{m}_F c_p/kL = 2.36$ and $L_f/L = 2.83$. To check, Eq. 4.4 predicts a total burning rate of $\dot{m}_F c_p/kL = 4.80$, which is composed of the top fueling rate $\dot{m}_{F,D} c_p/kL = 9.72 \times 10^{-2}$ and lateral fueling rate $\dot{m}_{F,L} c_p/kL = 4.71$. Also, the predicted flame height is $L_f/L = 4.38$. The calculated dominance of lateral fueling rate over top fueling rate is not unexpected given the 12/1 D/L ratio of the wick. The results, although coarse, demonstrate that Eq. 4.4 calculates burning rates and flame lengths that are order-of-magnitude correct but too high by 103% and 55%, respectively, on this single data point.

A minor component of the disagreement can be attributed to the low lateral fuel consumption rate, plotted in Fig. 4.2. That is, the lateral fuel consumption rate as predicted with $C_1 = 6.9$ following the method of LeFevre and Ede [32] is also too low by perhaps a factor of two. The constant C_1 can be adjusted if velocity data are available or a sensitivity analysis approach can be applied as in Fig. 4.3. The three lateral fuel consumption curves correspond to the original value of C_1, $2C_1$ and an upper limit of 20 above which the lateral burning rate exceeds the lateral supply rate for $B = 1$. It can be seen that each increase of C_1 increases the importance of burning lateral to the wick relative to burning above the apparent port burner. Selecting $C_1 = 0$ is nonphysical because such a choice implies that no oxygen is

present to combust fuel at the wick lateral region, yet a flame is present to vaporize fuel through the first term of Eq. 4.6.

The value assigned to C_1 is important because it effectively scales the axial velocity profile and therefore directly scales the upward mass flow term represented in Eq. 3.47. Consequentially, more fuel is predicted to be burned in the lateral region of the wick owing to increased air entrainment. Also, this corresponds to a reduction in the amount of fuel being transported to the apparent port burner and so flame heights will be shorter.

Even nearly tripling C_1 to a value of 20 has only a minor effect upon the apparent port burner flame height as shown in Fig. 4.8. From this, we conclude that that the majority of fuel burned in a candle does so in the overwick region. Intuitively, this can be understood as the result of increased air entrainment due to higher upward gas velocities produced by experiencing buoyant acceleration within the flame for a longer period. That is, fuel in the overwick region is moving faster because it has been accelerating over a longer period compared with the slow-moving fuel lower in the flame; these high velocities entrain more air and so have a higher burning rate.

One point of qualitative agreement between the flame length theory and experimental data is the absence of a strong trend due to the slenderness ratio, D/L. The theory predicts that the slenderness ratio plays a small role in determining the proportion of lateral- and top-vaporized fuel and that higher values of D/L should have taller flames, symbolizing that more fuel has been released from the top. Figure 4.8 shows that, overall, higher values of D/L do predict taller flames, but this effect is difficult to distinguish. Also, the wicks with the narrow range of $0.75 \leq D/L \leq 0.85$

exhibit flame lengths over nearly the entire range of measurements for other slenderness ratios. The theoretical curves for $D/L = 0.1$ and 1 should bound 30 of the 33 experimental data points, but they do not. It is likely that any effect from D/L is small as theory predicts, but is obscured in the experimental data because this effect is contained within measurement error.

More plausible explanations for the quantitative error lie within this thesis. One possibility is that the decision to use the material properties (k/c_p) of dry nitrogen introduces error, which could account for part of the fuel rate discrepancy as well. The unity Lewis number assumption for the mixture of hydrocarbons, products of combustion and air could contribute error. A nonunity Lewis number would affect the nature of the lateral burning rate math problem as well. Finally, the resultant equivalent diffusion rates may not be representative of the fuel in question, providing oxygen to the flame at a rate faster than expected, resulting in shorter flames. That is, axial diffusion of fuel towards oxidizer may be a non-negligible factor and one that causes more fuel to be burned at lower elevations than is predicted. Even with these discrepancies, however, we may assume from Roper's theoretical approach that overwick flame heights are proportional to the fuel rate supplied.

Chapter 5

Conclusion

A stagnant film model for characterizing the mass burning rate, length and width of the luminous region for candle flames was proposed and developed. In this analysis, radiation and sooting were ignored. The mass burning rate has been calculated by a heat transfer analogy in which empirical correlations based on the Rayleigh number were employed. The Rayleigh number is defined in terms of the temperature difference between peak flame temperature and the ambient, with material properties evaluated at the average temperature between the wick surface and flame sheet. The length of flames was estimated by modeling a circular port gaseous burner located immediately above the wick. The effects of curvature of the wick has been included by using a heat transfer correlation for cylinders.

The following assumptions were made:

1. The heat transfer from the flame to the wick can be modeled as a vertical cylinder at flame temperature cooling under the influence of natural convection without a surrounding flame front;

2. Pyrolyzate that has not burned laterally to the wick can be modeled as fuel flowing vertically from a circular port burner;

3. Compressibility effects can be ignored;

4. The flame and near flow field remain steady, laminar and axisymmetric;

5. The wick is shaped as a cylinder and remains uniformly saturated with liquid fuel at the surface; and

6. The fuel is burned in stoichiometric proportions with oxidizer.

Experimental flame lengths and widths were obtained for paraffin candles and compared with the model. Flame heights were overpredicted by approximately 170%. Flame widths were also overpredicted by approximately 100%. Both flame length and width followed the scaling trends predicted. However, the expected influence of the ratio of wick diameter to wick length was not seen in the experimental data; this may be phenomenological or this may be due to shortcomings in the photometric method of measuring candle flames.

5.1 Recommendations for Future Work

The following subsequent research is suggested.

1. A comparison of predicted and observed burning rates is warranted. Therefore, an inexpensive study in which candle mass loss is measured could be implemented to validate the mass burning rate model.

2. Comparison with the Alsairafi [26] or Raju [28] CFD models may provide mutual model validation.

3. National Institute of Standards and Technology's *Fire Dynamics Simulator* is

in the midst of releasing a new version. A study of candle flames using the liquid burning submodel may again provide mutual validation.

4. The experimental data bear out the fact that the unburnt and burning wick dimensions differ significantly. The change in wick dimensions can be studied by a photometric method. Wick porosity may play a role in the swelling or shrinking of the wick.

5. Photometric methods to measure flame and wick dimensions can be improved. In particular, several flame dimensions are difficult to discern in the visible spectrum. Alternate methods may lead to more precise measurements of candle flames.

6. This thesis assumed that the entire length of the candle wick was releasing fuel in a consistent way. However, the photographs show that there exists a region of wick near the wax pool that is below the flame. Here, the heat flux is lower than within the flame and consequently the vaporization rate is reduced. A study of the actual vaporization rate of this region or an analytical method of predicting it can be studied.

7. In contrast to the saturated conditions prescribed in this thesis, wicks may dry out near their tips, resulting in lower burning rates than predicted. This drying could be studied experimentally to determine the effect upon mass burning rate. Raju's [28] CFD model presents a computational approach to the question.

Appendix A
Summarized Measurements

No.	Relative to Pool			Diameters			
	Flame Height	Wick Length	Attachment	Flame	Wick (at top)	Wick (at Midpoint)	Dry Wick (via Caliper)
1.	5.81	2.39	0.85	3.92	0.92	0.68	0.81
2.	8.23	3.48	1.08	4.21	0.98	0.71	0.81
3.	9.40	5.66	1.50	4.57	1.09	0.74	0.81
4.	9.82	4.40	1.38	4.48	1.18	0.77	0.81
5.	10.81	6.74	1.60	4.68	0.63	0.82	0.81
6.	10.08	6.12	1.40	4.65	0.65	0.83	0.81
7.	13.23	7.47	1.65	5.19	0.94	1.13	1.10
8.	17.47	6.84	1.94	5.24	1.47	1.18	1.10
9.	14.24	5.67	1.96	5.07	1.58	1.24	1.10
10.	10.78	3.72	1.65	4.63	1.60	1.40	1.10
11.	8.31	3.07	1.15	4.33	1.60	1.40	1.10
12.	7.10	2.52	1.23	4.12	1.56	1.48	1.10
13.	7.16	2.70	1.33	4.13	1.57	1.51	1.10
14.	50.76	11.92	3.74	7.90	3.73	2.54	2.08
15.	51.90	9.61	3.24	7.84	3.86	2.65	2.08
16.	43.93	8.51	3.21	7.75	3.86	3.13	2.08
17.	26.07	5.67	2.26	7.25	4.52	3.62	2.08
18.	19.61	4.89	1.92	7.04	4.46	3.68	2.08
19.	36.35	6.99	2.56	7.54	4.25	3.69	2.08
20.	9.02	3.40	1.77	6.07	4.37	3.74	2.08
21.	20.24	4.66	2.06	6.36	3.30	2.86	2.58
22.	30.58	6.72	2.39	6.87	3.27	2.89	2.58
23.	50.55	9.99	2.33	7.69	3.30	2.89	2.58
24.	10.20	3.80	2.38	5.48	3.27	3.09	2.58
25.	7.99	3.68	2.36	5.21	3.19	3.12	2.58
26.	59.95	8.07	3.51	9.14	5.29	4.89	3.34
27.	44.22	6.13	2.65	8.66	5.31	4.91	3.34
28.	54.56	7.49	3.54	8.99	5.37	4.92	3.34
29.	14.30	3.21	2.10	7.34	5.40	5.04	3.34
30.	42.04	6.39	2.92	8.66	5.31	5.05	3.34
31.	34.71	6.13	3.19	8.63	5.32	5.07	3.34
32.	29.69	5.24	2.68	8.16	5.39	5.13	3.34
33.	21.46	4.10	2.10	8.01	5.38	5.22	3.34

Table A.1: Summary of data from candle flame experiments. Unit: mm.

Appendix B
Candle Flame Photographs

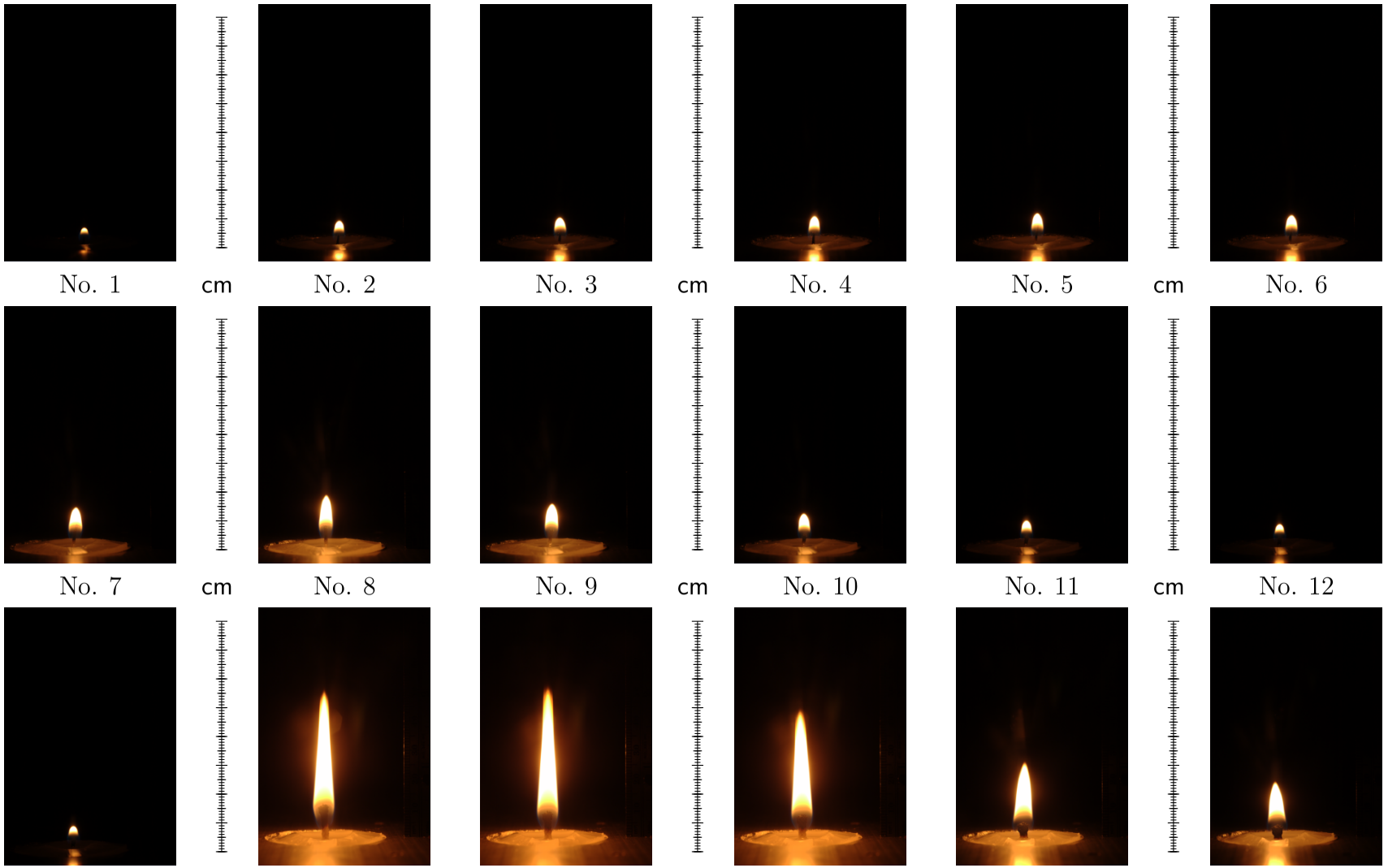
No. 1
cm
No. 2
No. 3
cm
No. 4
No. 5
cm
No. 6
No. 7
cm
No. 8
No. 9
cm
No. 10
No. 11
cm
No. 12
No. 13
cm
No. 14
No. 15
cm
No. 16
No. 17
cm
No. 18

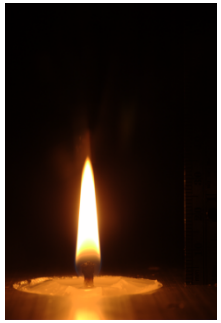
No. 19

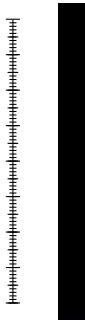
cm

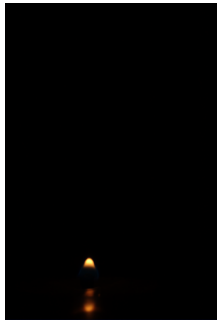
No. 20

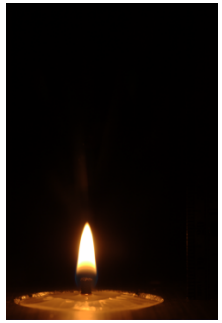
No. 21


cm

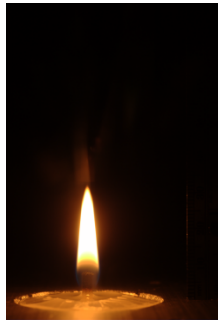
No. 22

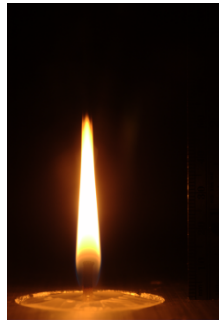
No. 23

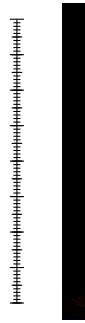
cm

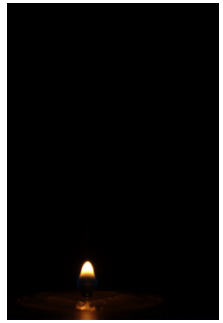
No. 24

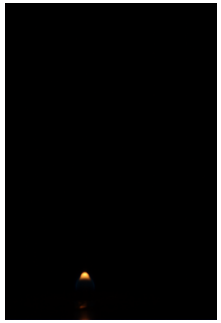
No. 25


cm


No. 26

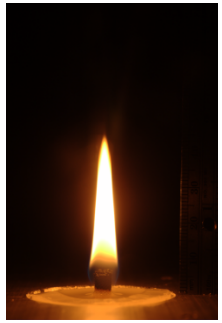
No. 27


cm

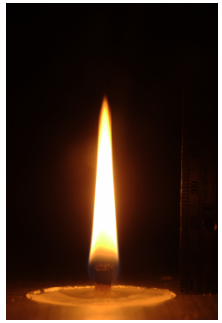
No. 28

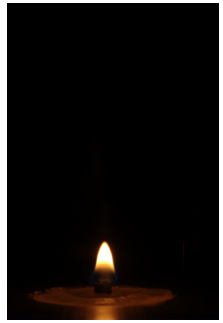
No. 29

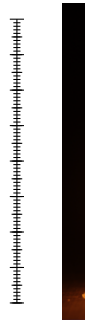
cm

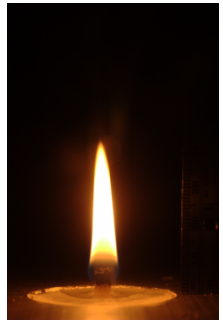
No. 30

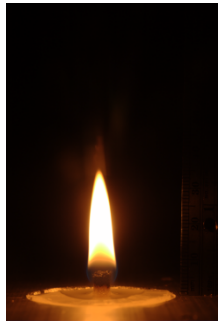
No. 31


cm

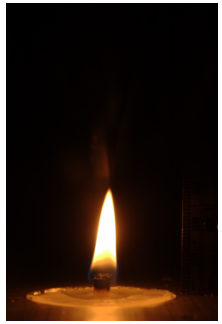
No. 32

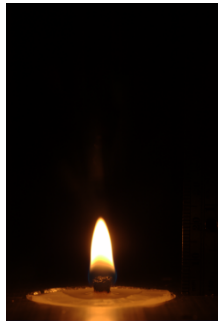
No. 33

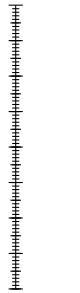
cm

Appendix C
Constants and Physical Values

Symbol	Value	Units	Comment	Source
B	4.29	-	Tetracosane at 298.15 K, see Eqn. 3.30	-
c_p (1)	1.053	kJ/kg·K	Nitrogen at 481 K (for B)	[42]
c_p (2)	1.199	kJ/kg·K	Nitrogen at 1169 K	[42]
C_1	6.9	-	$4\sqrt{105/\left(20+21\mathrm{Pr}\right)}$	-
k	0.074	W/m·K	Nitrogen at 1169 K	[42]
g	9.81	m/s^2	-	-
$\Delta h_c/s$	13,100	kJ/kg	-	-
H	-	-	See Table 3.1 for tetracosane	-
M_F	-	-	See Table 3.1 for tetracosane	-
M_∞	28.85	g/mol	-	-
Pr	0.72	-	-	-
Ra_x/x^3	3.50×10^8	m^{-3}	Ideal gas, $g\mu_m\left(T_f - T_\infty\right)/\mathrm{Pr}\,\alpha_m^2$	-
s	-	-	See Table 3.1 for tetracosane	-
S	-	-	See Table 3.1 for tetracosane	-
T_f	1673	K	Given as 1400 °C	[25]
T_v	664.5	K	Tetracosane	[43]
T_∞	298.15	K	-	-
$X_{\mathrm{Ox},\infty}$	0.21	-		-
$Y_{\mathrm{Ox},\infty}$	0.233	-		-
α	2.14×10^{-4}	m^2/s	Nitrogen at 1169 K	[42]
μ_m	8.56×10^{-4}	1/K	Ideal gas, $1/T_m = 2/\left(T_f + T_v\right)$	-

Notes:

1. 481 K is the average temperature between T_v and T_∞
2. 1169 K is the film temperature between T_f and T_v

Bibliography

[1] F. G. Roper, "The prediction of laminar jet diffusion flame sizes: Part i. theoretical model," *Combustion and Flame*, vol. 29, pp. 219–226, 1977.

[2] M. Faraday, *The Chemical History of a Candle*. Mineola, NY: Dover Books, 2002.

[3] H. W. Emmons, "The film combustion of liquid fuel," *Z. Angew. Math. Mech.*, vol. 36, pp. 60–71, 1956.

[4] D. B. Spalding, "Combustion of liquid fuels," in *4th International Symposium on Combustion*, (Baltimore, Md.), pp. 847–854, 1953.

[5] S. Abdel-Khalik, T. Tamaru, and M. M. El-Wakil, "An experimental and analytical determination of heat and mass transfer in a diffusion flame," in *Heat Transfer in Flames* (N. H. Afgan and J. M. Beer, eds.), pp. 365–374, Wiley, 1974.

[6] S. Abdel-Khalik, T. Tamaru, and M. M. El-Wakil, "A chromatographic and interferometric study of the diffusion flame around a simulated fuel drop," in *Proceedings of the 15th International Symposium on Combustion*, pp. 389–399, 1975.

[7] Y. Tao and M. Kaviany, "Burning rate of liquid supplied through a wick," *Combustion and Flame*, vol. 86, pp. 47–61, 1991.

[8] Y. Tao, M. Kaviany, and H. Merte, "Effect of wick surface saturation on evaporation rate in a forced convection diffusion flame," *Transactions of the ASME Journal of Heat Transfer*, vol. 96, pp. 35–43, 1988.

[9] M. Kaviany and Y. Tao, "A diffusion flame adjacent to a partially saturated porous slab: Funicular state," *Transactions of the ASME Journal of Heat Transfer*, vol. 110, pp. 432–436, 1988.

[10] M. Raju and J. S. T'ien, "Heat and mass transports in a one-dimensional porous wick driven by a gas-phase diffusion flame," *Journal of Porous Media*, vol. 10, no. 4, pp. 327–342, 2007.

[11] J. S. Kim, J. De Ris, and F. W. Kroesser, "Laminar free-convective burning of fuel surfaces," in *Proceedings of the 13th International Symposium on Combustion*, pp. 949–961, 1971.

[12] F. J. Kosdon, F. A. Williams, and C. Buman, "Combustion of vertical cellulosic cylinders in air," in *Proceedings of 12th Symposium of the Combustion Institute*, pp. 253–264, 1968.

[13] T. Ahmad and G. M. Faeth, "An investigation of the laminar overfire region along upright surfaces," *Transactions of the ASME Journal of Heat Transfer*, vol. 100, pp. 112–119, February 1978.

[14] S. F. Malary and M. Sibulkin, "Comparison of theoretical and experimental burning rates for a laminar wall fire," *Journal of Fire Sciences*, vol. 2, pp. 348–361, 1984.

[15] E. G. Groff and G. M. Faeth, "Laminar combustion of vertical free-standing fuel surfaces," *Combustion and Flame*, vol. 32, pp. 139–150, 1978.

[16] T. Maxworthy, "The flickering candle: Transition to a global oscillation in a thermal plume," *Journal of Fluid Mechanics*, vol. 390, pp. 297–323, July 1999.

[17] P. J. Pagni, "Diffusion flame analyses," *Fire Safety Journal*, pp. 273–285, 1980/1981.

[18] A. Linan, "Combustion of solid fuel cylinders under microgravity conditions," *Polymer Preprints, Division of Polymer Chemistry, American Chemical Society*, vol. 28, p. 461, 1987.

[19] D. L. Dietrich, H. D. Ross, Y. Shu, J. S. T'ien, and D. T. Frate, "Candle flames in microgravity," *NASA Conference Publication 10194*, pp. 237–242, 1997.

[20] D. L. Dietrich, H. D. Ross, J. S. T'ien, P. Chang, and Y. Shu, "Candle flames in non-buoyant atmospheres," *Combustion Science and Technology*, vol. 156, no. 1, pp. 1–24, 2000.

[21] W. Du, X. Zhang, I. Weim, W. Kong, and Y. Hua, "Candle flame temperature measurement in microgravity by differential interferometry (chinese)," *Journal of Combustion Science and Technology*, vol. 6, no. 2, 2000.

[22] H.-Y. Lyu and L.-D. Chen, "Numerical modeling of buoyant ethanol-air wick diffusion flames," *Combustion and Flame*, vol. 87, pp. 169–181, 1991.

[23] S. H. Wu and L.-D. Chen, "Numerical simulation of wick diffusion flames," *Journal of Propulsion and Power*, vol. 8, no. 5, 1992.

[24] N. Riley, "A sheet model for the candle flame," in *Proceedings of the Royal Society of London Series A: Mathematical and Physical Sciences*, vol. 442, pp. 361–372, 1993.

[25] A. Hamins, M. Bundy, and S. Dillon, "Characterization of candle flames," *Journal of Fire Protection Engineering*, vol. 15, pp. 265–285, 2005.

[26] A. Alsairafi, *A Computational Study On The Gravity Effect On Wick-Stabilized Diffusion Flames*. PhD thesis, Case Western Reserve University, May 2003.

[27] A. Alsairafi, S. T. Lee, and J. S. T'ien, "Modeling gravity effect on diffusion flames stabilized around a cylindrical wick saturated with liquid fuel," *Combustion Science and Technology*, vol. 176, no. 12, pp. 2165–2191, 2004.

[28] M. Raju, *Heat and Mass Transport Inside a Candle Wick*. PhD thesis, Case Western Reserve University, January 2007.

[29] J. G. Quintiere, *Fundamentals of Fire Phenomena*. John Wiley & Sons, Limited, 2006.

[30] K. M. Allan, J. R. Kaminski, J. C. Bertrand, J. Head, and P. B. Sunderland, "Smoke points of wax candles," *Combustion Science and Technology*, Accepted.

[31] S. Burke and T. E. W. Schumann in *First Symposium (International) on Combustion*, (Pittsburg, Pa.), pp. 2–11, 1928.

[32] E. J. Le Fevre and A. J. Ede, "Laminar free convection from the outer surface of a vertical circular cylinder," in *Proceedings of the 9th International Congress of Applied Mechanics*, vol. 4, pp. 175–183, 1957.

[33] S. R. Turns, *An Introduction to Combustion*. McGraw-Hill, second ed., 2000.

[34] A. M. Meirmanov, *The Stefan Problem*. Walter de Gruyter, 1992.

[35] E. M. Sparrow and J. L. Gregg, "Laminar-free-convection heat transfer from the outer surface of a vertical circular cylinder," *Transactions of the ASME Journal of Heat Transfer*, vol. 78, pp. 1823–1829, November 1956.

[36] O. G. Martynenko, Y. A. Sokovishin, and M. V. Shapiro, "Freely convective heat transfer at the external surface of a vertical isothermal cylinder," *Journal of Engineering Physics ad Thermophysics*, vol. 33, pp. 952–956, 1977.

[37] B. Gebhart, *Heat Transfer*. New York: McGraw Hill, 1971.

[38] F. G. Roper, C. Smith, and A. C. Cunningham, "The prediction of laminar jet diffusion flame sizes: Part ii. experimental verification," *Combustion and Flame*, vol. 29, pp. 227–234, 1977.

[39] P. B. Sunderland, B. J. Mendelson, Z.-G. Yuan, and D. L. Urban, "Shapes of buoyant and nonbuoyant laminar jet diffusion flames," *Combustion and Flame*, vol. 116, pp. 376–386, 1999.

[40] J. S. Chickos and J. A. Wilson, "Vaporization enthalpies at 298.15 k of the *n*-alkanes from c_{21} to c_{28} and c_{30}," *Journal of Chemical and Engineering Data*, vol. 42, no. 1, pp. 190–197, 1997.

[41] H. R. Nagendra, M. A. Tirunarayanan, and A. Ramachandran, "Free convection heat transfer from vertical cylinders and wires," *Chemical Engineering Science*, vol. 24, pp. 1491–1495, 1969.

[42] F. P. Incropera and D. P. De Witt, *Fundamentals of Heat and Mass Transfer*. John Wiley & Sons, second ed., 1985.

[43] R. C. Weast and J. G. Grasselli, eds., *CRC Handbook of Data on Organic Compounds*. CRC Press, Inc., second ed., 1989.